SEOM S1-4Sci Snow

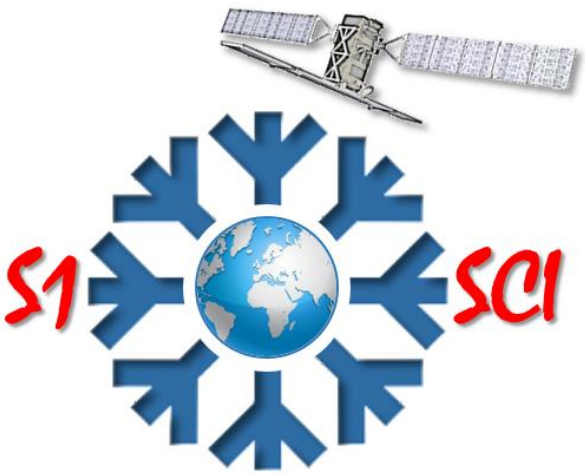

Development of Pan-European Multi-Sensor Snow Mapping Methods Exploiting Sentinel-1

Final Report

Deliverable 4.2

PRINCIPAL INVESTIGATOR: Thomas Nagler / ENVEO

PREPARED BY

Thomas Nagler, Gabriele Schwaizer, Lars Keuris and Helmut Rott, ENVEO IT GmbH, Austria

Kari Luojus and Mikko Moisander, Finnish Meteorological Institute, Finland

David Small, University of Zurich. Switzerland

Sari Metsämäki, Finnish Environment Institute, Finland

Eirik Malnes and Markus Eckerstorfer, NORUT, Norway

ISSUE / REVISION: 1.2

DATE: 20.02.2021

Document controlled by: [Thomas Nagler]

ESA STUDY CONTRACT REPORT

ESA CONTRACT NO:	SUBJECT:		CONTRACTOR:
4000118763	S1-4Sci Snow - Development of Pan-European Multi-Sensor Snow Mapping Methods Exploiting Sentinel-1 Final Report		ENVEO
ESA CR ( )NO:	**STAR CODE:**	**NO OF VOLUMES:** 1 **THIS IS VOLUME NO:** 1	**CONTRACTOR'S REF:** Deliverable 4.2

Multi-sensor snow mapping methods exploiting the Sentinel-1 combined with optical satellite sensors have been developed, implemented, tested, and evaluated over the Pan-European domain within the S1-4SCI Snow project. This document is the final report of the project and provides a concise overview on the methods and results as well as an outlook on further capabilities of the Sentinel-1 C-band SAR for the retrieval of new snow products.

The work described in this report was done under ESA Contract. Responsibility for the contents resides in the author or organisation that prepared it.

AUTHORS: Thomas Nagler, Gabriele Schwaizer, Eirik Malnes, David Small, Sari Metsämäki, Kari Luojus, Mikko Moisander, Lars Keuris, Markus Eckerstorfer, Helmut Rott

ESA STUDY MANAGER: Simon Pinnock / ESRIN	ESA BUDGET HEADING

This page is intentionally left blank.

DOCUMENT CHANGE LOG

Issue/ Revision	*Date*	*Modified pages*	*Modification*
1.0	20.11.2020	All	All
1.1	07.12.2020	-	Included comments by ESA
1.2	20.02.2021	Section 2	Some information added

This page is intentionally left blank.

TABLE OF CONTENTS

1. INTRODUCTION

1.1 Purpose

This document is the final report of the SEOM project S1-4Sci Snow – Development of Pan-European Multi-Sensor Snow Mapping Methods Exploiting Sentinel-1. The report provides an overview on the algorithm development exploiting Sentinel-1 (S1) and combing SAR and optical satellite data for monitoring snow for the Pan-European domain and on the evaluation and validation results of the S1 based wet snow products. It introduces the module "SAR Wet Snow Mapper" implemented in the frame of this project as toolbox extension for the ESA Sentinel Application Platform (SNAP), enabling also unexperienced SAR users to generate wet snow maps from S1 data, with the option to combine the approach with a snow map from optical satellite data. The document further includes a roadmap for improving upon available combined SAR optical snow products, as well as the scientific and technical research and development for monitoring other physical parameters of the seasonal snowpack using SAR data from past, current, and upcoming missions. The availability of archived SAR data for generating time series of snow products are elaborated, primarily focussing on ESA missions in the pre-Sentinel era.

The method for mapping wet snow using Sentinel-1 developed within this project is the basis for the SAR wet snow service implemented within the *Copernicus Land Monitoring Service - pan-European High Resolution Snow and Ice Service – Part II*.

1.2 Structure

This document is organized in 9 sections. After this introduction, the method and algorithm for mapping wet snow from S1 are described in Section 2. A method for combining optical and SAR satellite data for an improved snow product providing information on the snow extent and the snow state (dry / wet) and results of this approach tested for the Pan-European domain are presented in Section 3. The snow extent from optical satellite data has been evaluated in several other projects (e.g. ESA DUE GlobSnow, ESA S2-S3 Model Snow, EU FP7 CryoLand, Copernicus Land Monitoring Service). Thus, it was decided to focus on the validation of the S1 based wet snow product. The evaluation results of the wet snow product from S1 data are summarized in Section 4. The method for mapping wet snow from S1 data has been implemented in a SNAP module, which is described in Section 5. Potential advances of SAR and combined SAR/Optical snow products are discussed in Section 6. Ideas to exploit the SAR capabilities for retrieving new snow products are provided in Section 7. To generate historic time series of wet snow products, the availability of ENVISAT ASAR data over the Pan-European domain was investigated and is described in Section 8. Section 9 lists all references.

1.3 Acronyms

ASAR	Advanced SAR onboard of ENVISAT
CA	Cultivated Areas
CoReH$_2$0	COld REgions Hydrology High-resolution Observatory, Earth Expl. 7 Candidate Mission
D	Dozier and Painter, 2004
DF	Dense Forest
DInSAR	Differential SAR Interferometry
DMRT	Dense Medium Radiative Transfer
ENVISAT	Environmental Satellite
ERS	European Remote Sensing Satellite
FAR	False Alarm Rate
FSC	Fractional Snow Cover
HBV	Hydrologiska Byråns Vattenbalansavdelning model
IEM	Integral Equation Model
IM	Image Mode
InSAR	Interferometric SAR
IWS	Interferometric Wide Swath mode
K	Klein *et al.*, 1998
L	Lowlands
LST	Land Surface Temperature
LWC	Liquid Water Content
M	Mountains
MODIS	Moderate resolution Imaging Spectroradiometer
NVE	Norwegian Water Resources and Energy Directorate
QA4EO	Quality Assurance framework for Earth Observation
RCM	Radarsat Constellation Mission
RRE	Round Robin Exercise
S	Salomonson and Appel, 2006
S1	Sentinel-1
SAR	Synthetic Aperture Radar
(S)BF	(Sparse) Boreal Forest
SD	Snow Depth
SI	Snow Index
SNAP	Sentinel Application Platform
SnowPEx	Satellite Snow Products Intercomparison and Evaluation Exercise

SWE	Snow Water Equivalent
THR	Threshold
V_w	Liquid Water Content
WCOM	Water Cycle Observation Mission, Chinese Satellite Mission
WSFS	Watershed Simulation and Forecasting System
WSM	Wide Swath Mode
ZAMG	Zentralanstalt für Meteorologie und Geodynamik, Austrian Weather Service
σ^0	backscatter coefficient
θ	local incidence angle
R_c	backscatter ratio, combined
R_{vh}, R_{vv}	cross-, co-polarized backscatter ratios

2. SAR WET SNOW MAPPING ALGORITHM

This section describes the algorithm for detecting melting snow using dual polarization S1 backscatter data. For algorithm development the results of the round robin exercise of wet snow mapping algorithms of ENVEO, NORUT and UZH carried out within this project are considered.

2.1 Physical background of wet snow detection using SAR

The reduced backscattering coefficient (σ^0) of wet snow compared to surfaces that are snow-free or covered by dry snow provides the basis for mapping snowmelt areas (e.g. Nagler and Rott, 2000; Mätzler 1987). Due to the high dielectric losses of liquid water, σ^0 of snow decreases with increasing liquid water content. The typical C-band one-way penetration depth of dry seasonal snow is about 20 m, whereas for wet snow with liquid water content of 5 % by volume, it is only 3 cm (Mätzler 1987). Whereas for wet snow the radar signal at C- and X-band frequencies is reflected and scattered at the surface and within the uppermost centimetres of the snowpack, in the case of dry seasonal snow, a main part of the observed signal is contributed by the snow/ground interface. Consequently, the contrast in backscatter intensity of dry snow areas and snow-free surfaces is small and not suitable for reliable mapping of dry snow.

The backscatter intensity of wet snow is subject to temporal variations, which may affect the snow retrievals. Refreezing of the surface layer, for example during a cloudless night, might cause an increase in σ^0 due to the high scattering albedo of the frozen layer (Floricioiu and Rott, 2001). This results in a decrease in the contrast of snow *versus* snow-free surfaces. Backscatter theory and experimental data show that this effect is less pronounced at C-band than at X-band because of the smaller scattering efficiency and the better penetration through the frozen layer at the longer wavelength (Floricioiu and Rott, 2001).

Another issue that plays a role for snow retrievals is the angular dependence of backscatter. The backscatter contrast between melting snow and snow-free surfaces changes with the local incidence angle of the radar beam, which refers to the normal surface. For co-polarized backscatter, the contrast in σ^0 decreases significantly towards low incidence angles because of a comparatively strong rise of the backscatter signal of wet snow surfaces. Cross-polarized backscatter shows less angular dependence, maintaining a clear difference between wet snow and snow-free surfaces at low incidence angles. On the other hand, at high incidence angles cross-polarized backscatter may approach the noise floor. For these reasons, it is advisable to use both the co- and the cross-polarized channel for snow retrievals if available.

2.2 Round-robin-exercise of wet snow mapping algorithms

As starting point for the wet snow algorithm development, a Round-Robin-Exercise (RRE) with different wet snow retrieval approaches available at the different project partners was performed. The round-robin test sites (Figure 2.1) were selected regarding different environments in Europe:

- mountainous/alpine areas (Austrian and Swiss Alps, Northern Scandinavia),
- sparse forest and tundra, lowlands (Finland), and
- cultivated areas and dense forested areas, lowlands (Poland).

Figure 2.1: Location of round robin test sites in Europe.

Wet snow products generated by four different project partners with different wet snow detection algorithms applied on S1 data were intercompared with each other and further validated with reference snow maps from high resolution optical satellite data from Sentinel-2 (S-2) and Landsat-8. For the generation of the reference snow maps, three different algorithms were applied: (D) Dozier and Painter (2004), resulting in binary snow maps; (K) Klein *et al.* (1998), resulting in binary snow maps; and (S) Salomonson and Appel (2006), resulting in fractional snow maps. Only one approach, the wet snow algorithm of ENVEO, was applied in all cases. The statistical measures Cohen's κ-coefficient and the total accuracy between each product comparison are shown in Table 2.1. As expected, the highest κ-coefficients and best agreement of products are found for mountainous regions, the lowest for forested and cultivated areas. The validation of the wet snow maps with reference snow maps from high resolution optical satellite data shows also the highest κ-coefficients and best overall accuracy for mountainous regions. This is expected, as the wet snow detection algorithms were originally developed for application in high alpine/mountainous terrain. But larger differences are found for lowlands and for scenes including forested areas, as illustrated in Figure 2.2, left image. Difference

maps of the wet snow maps from different partners (Figure 2.2, right) are used to investigate the regional differences and capability of detecting wet snow regarding different surface classes. Based on the validation results and the fact that only the algorithm of ENVEO was tested and intercompared for all surface classes all over Europe, this approach is selected as baseline algorithm.

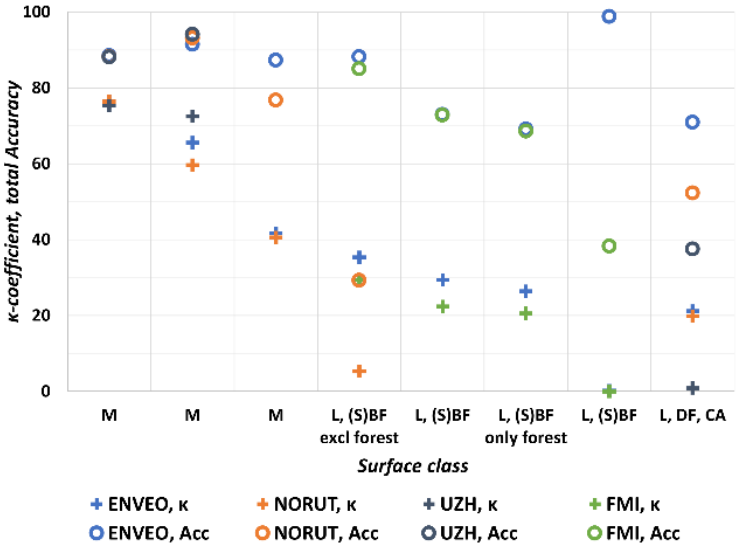

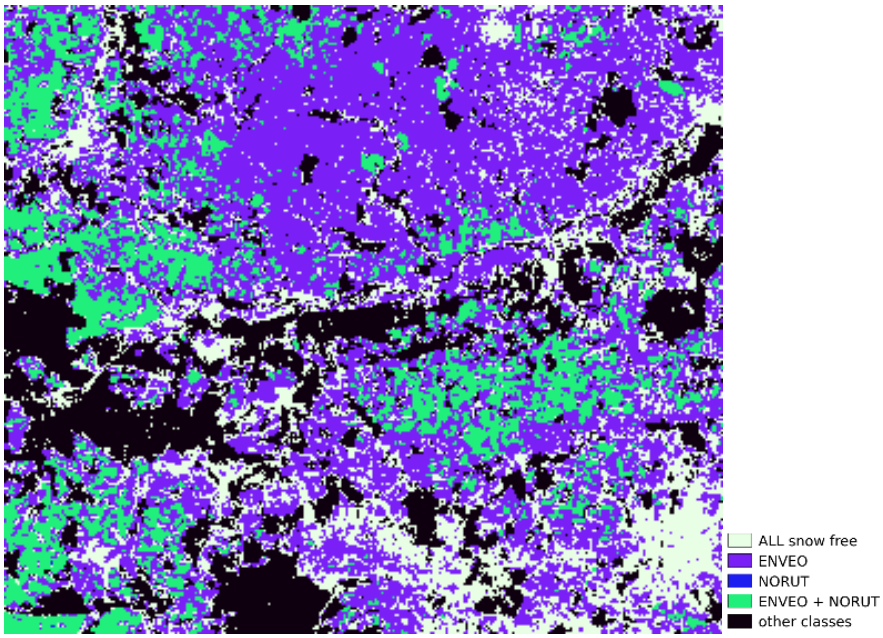

Figure 2.2: Left: κ-coefficient and total accuracy per RRE test site and surface class (abbreviations see Table 2.1) evaluated with reference snow maps from Landsat generated with the algorithm of Salomonson and Appel (2006). Right: Difference maps of wet snow maps from S1 generated by ENVEO and NORUT, subset of 16 February 2016 (region 3, surface classes L, DF, CA).

Table 2.1: κ-coefficient and total accuracy of wet snow product intercomparison from different algorithms for selected test sites (cf. Figure 2.1), covering different surface classes in Europe. E=ENVEO, N=NORUT, U=UZH, F=FMI.

Date	Surface class*	Region ID	κ-coefficient				Total Accuracy			
			E vs N	U vs N	E vs U	E vs F	E vs N	U vs N	E vs U	E vs F
28.04.2016	M	1	22,0	--	--	--	73,9	--	--	--
30.04.2016	L, (S)BF, incl. forest	2	--	--	--	0,8	--	--	--	71,0
30.04.2016	L, (S)BF, excl. forest	2	10,4	--	--	--	45,4	--	--	--
12.05.2016	L, (S)BF, incl. forest	2	--	--	--	2,6	--	--	--	73,5
16.02.2016	L, DF, CA	3	4,1	--	0,2	--	31,7	--	7,2	--
28.06.2016	M	4	66,9	78,2	63,4	--	93,6	96,2	92,8	--
04.05.2016	M	5	82,0	85,9	85,9	--	91,0	93,0	93,0	--
Mean			**37,1**	**82,1**	**49,8**	**1,7**	**67,1**	**94,6**	**64,3**	**72,3**
Number of cases			5	2	3	2	5	2	3	2

* M = mountains, L = Lowlands, (S)BF = (Sparse) Boreal Forest, DF = Dense Forest, CA = Cultivated Areas.

2.3 Overview of the SAR snow mapping algorithm

The flow chart of the baseline algorithm for SAR snowmelt area mapping is shown in Figure 2.3 (Nagler *et al.*, 2016; Nagler and Rott, 2000). It makes use of the enhanced imaging capabilities of S1 Interferometric Wide swath (IWS) mode featuring dual-pol (VV, VH) acquisitions. The algorithm applies change detection by intercomparing the wet snow images versus the reference images which represent typical backscatter conditions of terrain which is snow free or covered by dry snow covered (which is transparent at C-band).

Calibration of S1A and S1B data is applied to allow the use of multi-sensor data and to increase temporal observation frequency. The SAR backscatter images are affected by speckle. Speckle is reduced by multi-looking the single SAR acquisitions, and by applying a multi-channel (or multi-temporal) SAR speckle filter. To exploit the dual-polarisation capabilities of S1 we calculate the ratio of the snow versus the reference data for co – and cross-polarisation separately and combine the two ratio values making accounting for differences in angular backscatter behaviour of co- and cross-polarized backscatter data. After geocoding, segmentation of wet snow is performed by applying a threshold value on the combined VV and VH backscatter ratio image. Post-processing is applied to correct for areas where changes of backscatter are not related to snow melt but to other processes, as for example changes in soil moisture, vegetation growth, and agricultural activities. The post-processing rules are dependent on the land cover and terrain, and therefore are different for

mountainous areas and lowlands. This processing is carried out for S1 tracks separately, providing a dedicated time stamp on the dataset. Different tracks acquired on the same day or within a period of a few days can be merged to obtain the snow melt maps over large areas.

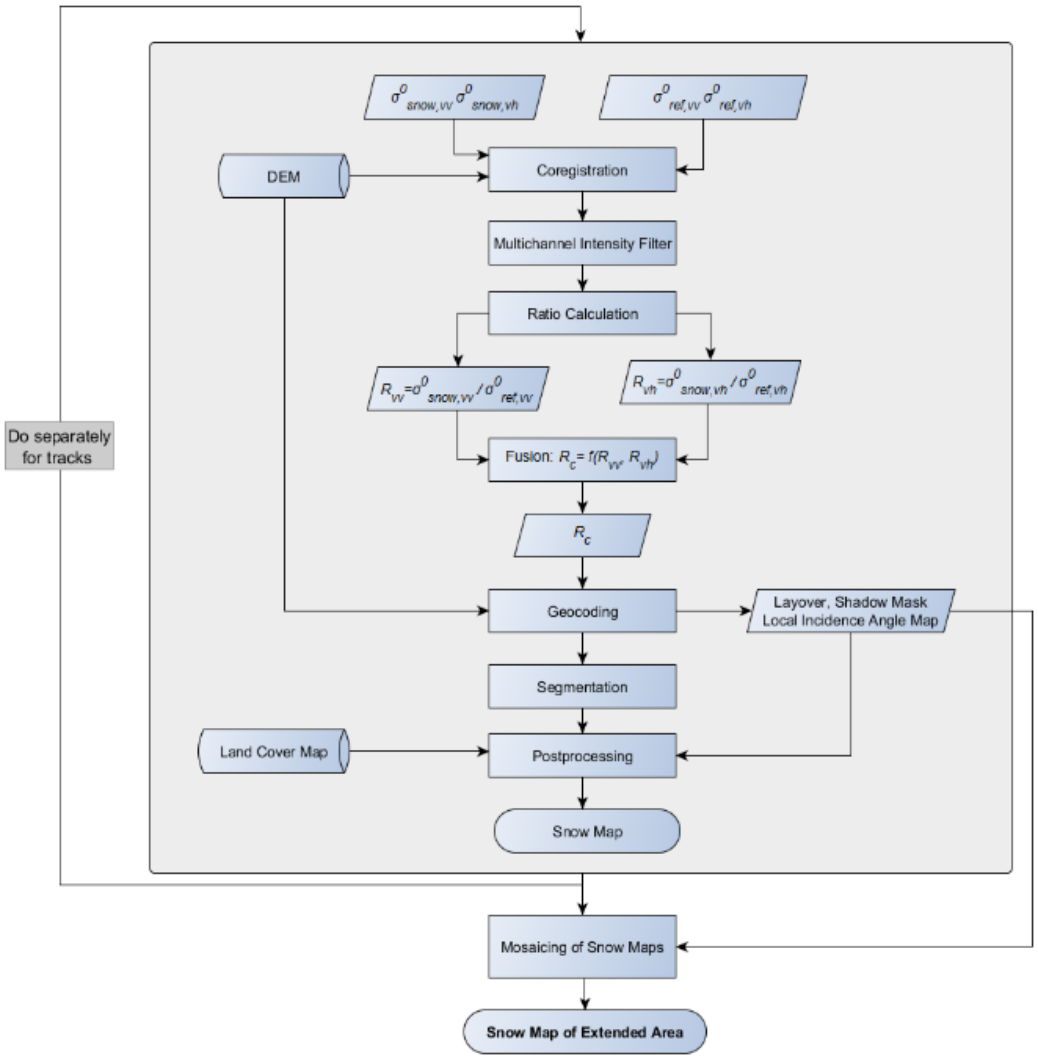

Figure 2.3: Processing line of SAR wet snow algorithm using co- and cross-pol S1 IWS SAR data.

In the following subsections, only the processing steps for generating the reference image and the wet snow maps for the Pan-European domain are described. All further technical steps are described in detail in the Algorithm Theoretical Basis Document (SEOM S1-4SCI Snow, Del. 2.1).

2.4 Generation of reference image

In the context of SAR wet snow mapping reference images represent characteristic backscatter of the snow free ground, preferable during winter conditions. As dry snow is transparent at C-band, snow

free images and images acquired during winter with dry snow conditions from the late autumn are combined to form the reference image. In the case of regional to continental products long data tracks of more than 1000 km length are processed covering different environments and climate zones with different surface conditions. We developed and implemented locally adaptive multi-temporal procedures with the aim to select suitable surface conditions to calculate the reference backscatter value on a pixel-by-pixel basis. This is done by statistical analysis of a time series of co-registered S1 images for each pixel of more than 30 acquisitions.

Three approaches were tested for the generation of the reference image, (1) single acquisition, (2) average of several manually selected reference images (Nagler and Rott, 2000), and (3) pixel wise statistical analysis of time series of reference images (only rough selection).

For regional to continental SAR wet snow processing the pixel-wise statistical analysis of a time series of SAR images has been selected to generate the reference image (see Figure 2.4). The following steps are applied separately for co- (VV) and cross-polarized (VH) images:

- generate a single-master stack of about 30 or more SAR repeat pass SAR images
- Extract the time series for each pixel and sort values in decreasing order of backscatter. The reference backscatter value for each pixel can be derived by various options:
  - Option 1: calculated by average backscatter value: suitable if only a few SAR images are available, which does not allow a statistical analysis per pixel
  - Option 2: calculate average of all backscatter values between highest 5 values (not recommended as sensitive to outliers in backscatter).
  - Option 3: apply outlier removal and calculate the average of the upper quartile of the backscatter values per pixel (requires sufficient number of images, e.g. more than 30 images).

Due to the high frequency of S1 SAR acquisitions over Europe (continuously 6 days repeat track acquisitions) we recommend using Option 3.

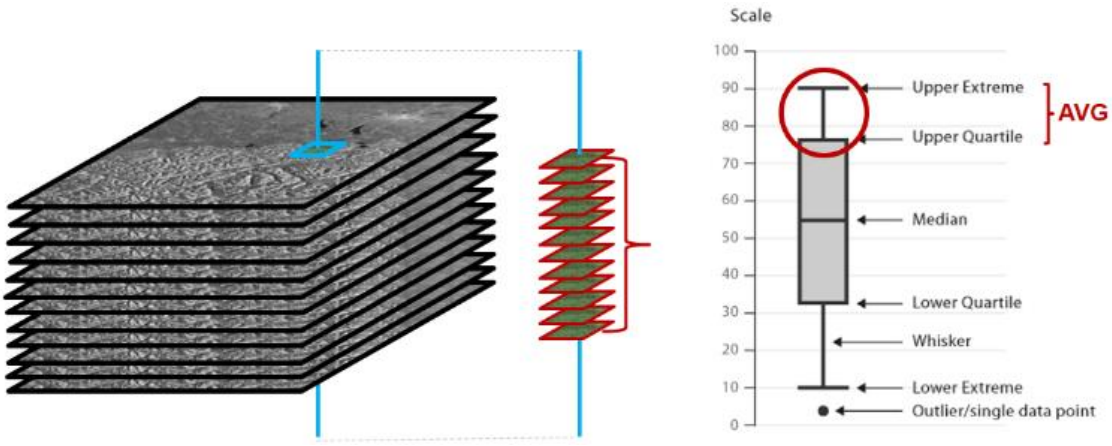

Figure 2.4: Generation of a multi-temporal pixel wise reference image (AVG – Average).

2.5 Calculation of backscatter ratio and fusion of co- and cross-polarized data

Segmentation of snowmelt areas is done in SAR image geometry utilizing the ratio of the snow versus the reference image. The co- and cross polarized ratios, R_{vv} and R_{vh}, are calculated according to

$$R_{vv} = \frac{\sigma^0_{vv,snow}}{\sigma^0_{vv,,ref}} \qquad \textit{Eq. 2.1}$$

and

$$R_{vh} = \frac{\sigma^0_{vh,snow}}{\sigma^0_{vh,,ref}} \qquad \textit{Eq. 2.2}$$

The backscatter ratios of snow-free surfaces and dry snow areas show small temporal variations, whereas the backscatter ratios of melting snow may change in time. Taking into account this angular behaviour (Nagler *et al.*, 2016) , we apply the following relation for merging R_{vv} and R_{vh} ratios in order to create a combined single channel, R_c:

$$R_c = W\, R_{vh} + (1 - W)\, R_{vv} \qquad \textit{Eq. 2.3}$$

The weight (W) varies with the local incidence angle (θ) applying the following rule:

$$\begin{aligned} &IF\ (\theta < \theta_1) && \rightarrow\ \{W = 1.0\} \\ &IF\ (\theta_1 \le \theta \le \theta_2) && \rightarrow\ \left\{W = k\left[1 + {(\theta_2 - \theta)}\Big/{(\theta_2 - \theta_1)}\right]\right\} \\ &IF\ (\theta > \theta_2) && \rightarrow\ \{W = k\} \end{aligned} \qquad \textit{Eq. 2.4}$$

We use $k = 0.5$, $\theta_1 = 20°$, $\theta_2 = 45°$. This means that R_{vv} and R_{vh} have the same weight for $\theta \geq 45°$. For $\theta < 45°$ the weight of R_{vv} decreases gradually, vanishing at $\theta = 20°$. We limit the local incidence angles for snow mapping to the range $15° \leq \theta \leq 75°$. At lower angles the surface resolution in range decreases significantly. At higher incidence angles the signal-to-noise ratio for targets with low reflectivity such as wet snow is quite small. Besides, for steep fore-slopes and near-grazing incidence possible errors in the DEM used for geocoding become critical.

2.6 Segmentation and post-processing

To remove outlier pixels, we apply a median filter with 3x3 filter window size on the geocoded R_c ratio image. Segmentation of wet snow applies a threshold of THR = -2 dB to the geocoded filtered R_c ratio image. The selection of this threshold value is based on histograms of the ratio values of the two classes derived for different mountainous environments where snow reference data sets are available and are confirmed by Round Robin Exercises (see Section 2.2). Additionally, we use a land cover map to exclude dense forests and open water surfaces.

The wet snow product is generated by applying for mountain areas the following rules on the filtered geocoded R_c ratio image pixel-by-pixel. For different environments and surface classes the rules need to be adapted:

$$
\begin{aligned}
&IF\ Layover && \rightarrow\ Class:\ Invalid \\
&ELSE\ IF\ Shadow && \rightarrow\ Class: Invalid \\
&ELSE\ IF\ \theta_i < 15° \ or\ \ \theta_i > 75° && \rightarrow\ Class: Invalid \\
&ELSE\ IF\ OpenWater && \rightarrow\ Class: OpenWater \\
&ELSE\ IF\ Forest && \rightarrow\ Class: Forest \\
&ELSE\ IF\ (R_c < THR) && \rightarrow\ Class: WetSnow \\
&ELSE && \rightarrow\ Class: Snowfree - orDrySnow
\end{aligned}
\qquad \textit{Eq. 2.5}
$$

2.7 Mosaicking of snow melt products from multiple tracks

For generating snowmelt extent maps for large areas, such as the Pan-European domain, data from multiple S1 tracks are combined, using two or more snow products from different tracks in the same map projection. For merging the optimal resolution approach is applied, using the classification result from the track with the best local resolution for a pixel (which means with the higher local incidence angle). Layover and shadow areas, fore-slopes and steep backslopes are masked out.

If several tracks from different several days are merged, a pixel can be covered by multiple observations at different acquisition times. In this case we calculate the fraction of observations where the pixel is classified as wet snow, providing information on the consistency between observations of different tracks.

3. PAN EUROPEAN COMBINED SAR AND OPTICAL SNOW PRODUCT

3.1 Introduction

In areas with close to 100 % snow coverage during winter it can be assumed that backscatter changes are caused by snow melt. However, temporal backscatter changes may result from other processes, for instance in areas with agricultural activity (Figure 3.1). Dense forest cover is a major obstacle for snow detection by SAR. Therefore, areas with dense forest cover are masked out. For mapping snowmelt area by SAR change detection in areas with agricultural activity (Figure 3.2 and Figure 3.3) ambiguities need to be checked, using the combination of optical and SAR snow classification.

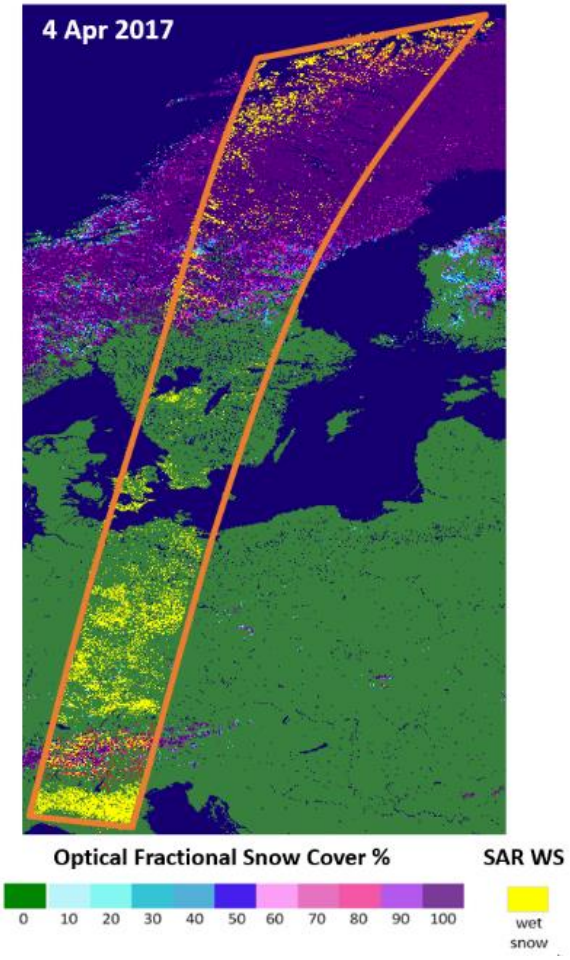

Figure 3.1: Example of optical fractional snow cover map overlaid with S1 based snowmelt map (yellow), both from 4 April 2017. Wet snow and dry snow can be clearly identified in mountainous areas of the Alps and Scandinavia. Ambiguities in SAR wet snow detection are visible in the Po Valley in Italy, and in Germany, where changes in backscatter are mainly caused by agricultural activity and changes in soil moisture.

Figure 3.2: Agricultural fields in the Po valley, Italy, revealing flooded rice fields with variable water level.

Figure 3.3: Agricultural fields in Central Germany with different crop types and vegetation stages showing the spatial complexity and variability.

3.2 Method for merging for optical FSC and SAR melt extent product

The snow and melt extent product for the Pan-European domain provides information on the total snow extent and melt areas and is derived from the synergistic use of SAR and optical snow products. The following steps are applied to combine snow maps from both sources:

- **Step 1:** Apply cloud-clearing to optical FSC map: we use the prototype method for assimilation of optical FSC products with a snowpack model driven by output from numerical meteorological models. Current optical FSC products have a pixel spacing between 250 m and 1 km (Schwaizer *et al.*, 2019).
- **Step 2:** Transform SAR snowmelt map (100 m x 100 m pixel spacing) into map projection of optical FSC map.
- **Step 3:** Combine wet snow and optical FSC maps: as a pre-condition for the presence of wet snow from SAR data, the FSC in the optical snow product should have nearly close snow cover (**FSC > THR**). We propose a threshold of THR = 90%. The threshold has been derived by intercomparison with snow reference data.
- **Step 4:** Exclude open water and dense forests areas, where wet snow detection does not work, by using a land cover and open water mask.

An example of the merged optical FSC map and SAR based melt extent for Scandinavia on 20 April 2018 is shown in Figure 3.4. The SAR based melt extent is shown in yellow and is overlaid to the FSC map from optical data from the same day. Forested areas are masked in the snow product. Figure 3.5 shows the multitemporal snow cover and melt extent product for the Pan-European domain, using S1 IWS tracks for the period and corresponding optical FSC maps from the same day. In the northern part of Scandinavia, the variable melt conditions during the acquisition of different S1 overflights are visible.

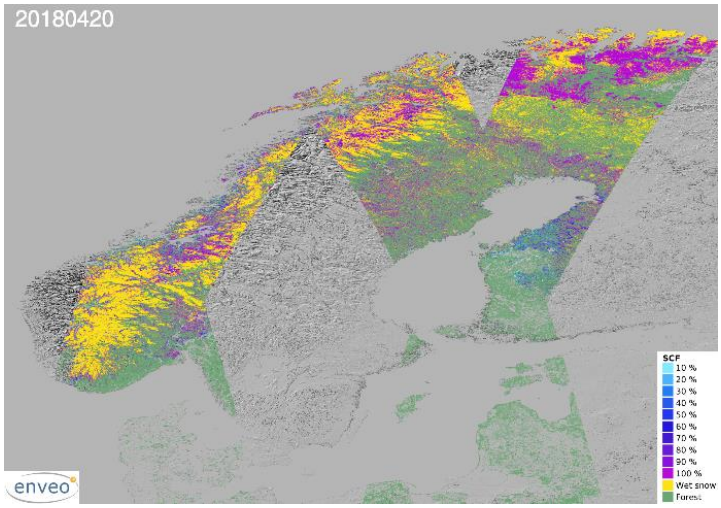

Figure 3.4: Snow cover and melt extent product from medium resolution optical satellite data and S1 SAR data, for Scandinavia, 20 April 2018. Forests – green; Back-ground – hill-shaded DEM.

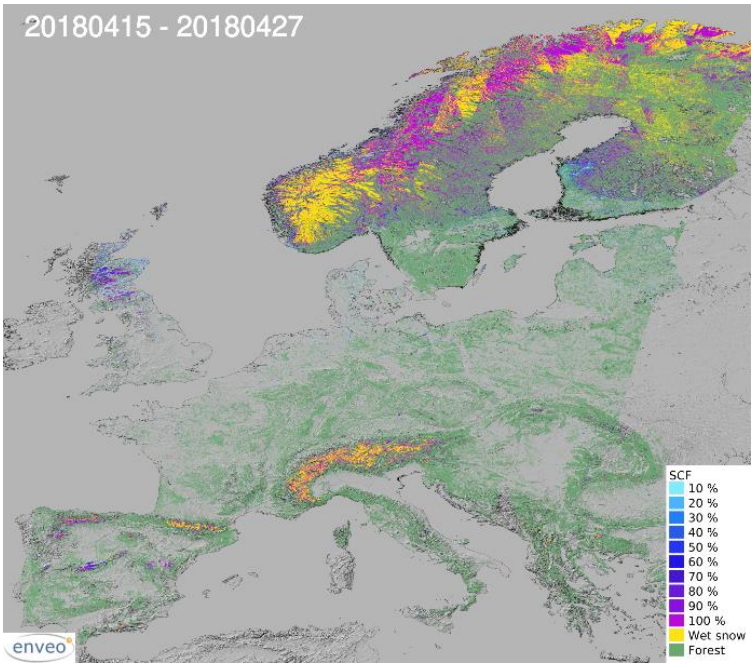

Figure 3.5: Snow cover and melt extent product from medium resolution optical satellite data and S1 SAR data, for Pan-European domain, for the period 15 to 27 April 2018.

4. VALIDATION OF SAR WET SNOW PRODUCT

For validating the SAR based wet snow products, reference snow information from different sources is used:

- Snow maps from high-resolution optical satellite images (Landsat-8, Sentinel-2) acquired nearly coincidently with the SAR images during the melting seasons 2017 and 2018.
- In-situ snow depth observations combined with observations on ground status (called e-codes), reported at European weather stations from January to June 2017
- In-situ snow depth observations combined with the land surface temperature (LST) dataset from MODIS/Aqua (MYD11A1) and MODIS/Terra acquisitions (MOD11A1) provided by NASA.
- Output of hydrological models available for Finland (melt rate and snow water equivalent) and southern Norway (liquid water content)

4.1 Preparation of reference data

4.1.1 Reference snow maps from high resolution optical satellite data

Reference snow maps for the validation of wet snow maps from S1 data are based on 69 high resolution optical satellite data acquired mainly at cloud free conditions in the melting seasons 2017 and 2018 in different mountainous regions of the Pan-European domain. The preparation of the reference snow maps from high resolution optical satellite data follows the guidelines defined in the ESA Quality Assurance framework for Earth Observation (QA4EO) project Satellite Snow Products Intercomparison and Evaluation Exercise (SnowPEx) (Ripper *et al.*, 2019). The reference snow maps using different snow algorithms (Salomonson and Appel, 2006 (S), Klein *et al.*, 1998 (K), Dozier and Painter, 2004 (D)), as described in Ripper *et al.* (2019), are generated at the original pixel size of the sensors (30 m for Landsat, 20 m for Sentinel-2), and then aggregated to a fractional snow cover information at the pixel size of the wet snow products (100 m). For validating the binary wet snow information, the aggregated fractional snow cover maps are converted to binary snow information, testing different thresholds (25%, 50%, 75%, 90% and 100% FSC). The Salomonson and Appel (2006) algorithm (2006) approach with a threshold of 90% snow cover fraction resulted most frequently in the highest κ-value and total accuracy values. Thus, the validation results are presented using this threshold (90% FSC) for the conversion of the reference snow maps into binary snow information. For the validation of the S1 wet snow products at 100 m grid size, 58’333’312 pixels are used per reference snow algorithm (S, K, D) applied on the high-resolution optical satellite data.

4.1.2 Snow depth and e-code data

For the validation with in-situ snow observations, snow depth measurements are combined with the observations of the ground status, considering reported “wet/compact full snow cover” (Finnish weather stations e-code 7, other European stations, e-codes 13 and 14) and “dry snow” (Finnish weather stations e-code 9, other European stations e-codes 15 and 16). As 75% of the European stations reported “wet snow full coverage” even if snow depth is 0 cm, only those e-codes with concurrent snow depth ≥ 5 cm were accepted in the reference dataset. The remaining observation points are used for the validation of 189 wet snow products from S1 at 100 m grid size. Thereby, only wet snow products from S1 ascending tracks, i.e. only afternoon acquisitions were considered. In total, 4727 comparison pairs are available for the wet snow product validation with e-codes and snow depth data (>5cm).

4.1.3 Land surface temperature and snow depth data

The LST data are based on MODIS/Aqua acquisitions (MYD11A1) and MODIS/Terra acquisitions (MOD11A1), providing daily per-pixel temperature for cloud free pixels. Separate day and night grids for the entire Pan-European domain for the period January to June 2017 are used for the validation activities. The LST grids are combined with snow depth (SD) information from weather stations, using snow depth of 2 cm to label weather station location as ‘snow covered’, to discriminate wet and dry snow status. After an extensive analysis of the relations between day and night LST, snow depth measurements and snow status reported by e-codes, a set of criteria has been elaborated (Figure 4.1) to classify a pixel based on LST and snow depth data as snow free, dry snow, or wet snow. For the validation of the S1 based wet snow product at 100 m grid size, 659 comparison pairs with in-situ snow depth data and LST data are used.

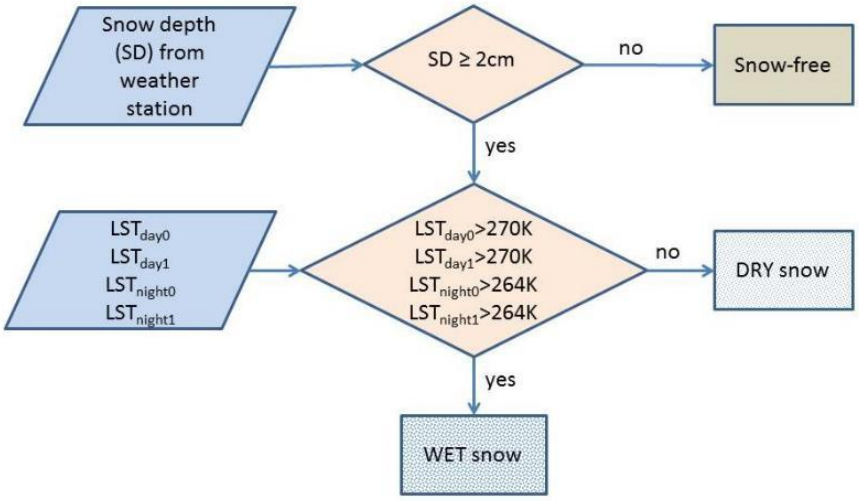

Figure 4.1: The scheme for wet snow identification from Land Surface temperature field and Snow depth observed at weather stations.

4.1.4 Output from hydrological models

The output of hydrological models driven by precipitation and temperature from meteorological models and calibrated against runoff in rivers and reservoirs are used for validation activities. Products from two models are available for comparison activities: (i) The Watershed Simulation and Forecasting System (WSFS) of SYKE, and (ii) the HBV hydrological model operated by the Norwegian Water and energy directorate (NVE).

The WSFS model of SYKE produces daily gridded data with 1 km pixel spacing on snow melting rate [mm/day] and Snow Water Equivalent [mm] for Finland. The output of the WSFS is resampled to the pixel spacing of the wet snow product (100 m). The melt rate and SWE are used to classify the model grid as wet snow or drysnow/snowfree:

IF SWE > 80mm AND melt rate > 2mm/d THEN wet snow, OTHERWISE dry snow/snow free

The S1 based wet snow product at 100 m grid size is compared on a pixel-by-pixel basis with modelled wet snow resulting from hydrological models in Finland.

The calibrated degree-day hydrological model HBV operated by NVE provides daily estimates of Liquid Water Content (LWC) in % for a distributed grid with 1 km spatial resolution over the entire Norway and some of the surrounding territories in Sweden and Finland. The model is used to evaluate the wet snow detections from S1, aggregating the S1 wet snow products to the 1 km grid of the HBV output. To convert the LWC of the hydrological model HBV in southern Norway with 1 km grid size into wet snow information and compare it with the aggregated wet snow maps from S1, different threshold combinations were tested. Finally, for the model output a threshold of LWC>5% is used, and for the aggregated wet snow products a threshold of 10% is applied. Three different levels of comparisons were performed with the HBV model output for southern Norway:

- *Multi-temporal analysis:* daily wet snow products from S1 for the full years 2017 and 2018 are analysed and compared with the daily averaged modelled LWC at 1 km resolution.
- *Single day analysis:* daily wet snow products from S1 are compared pixel-by-pixel with daily averaged modelled LWC maps at 1 km resolution.
- *Diurnal variability analysis:* wet snow products from ascending and descending S1 swaths acquired in the morning and the afternoon of the same date are compared with the LWC model output sampled every 3 hours instead of the daily average. This high temporal resolution product of the HBV model is available from mid of April 2018 until March 2019 and is compared with all available single swath wet snow products from S1 for this period.

4.2 Validation results

The S1 based binary wet snow products covering the Pan-European domain were validated with the reference snow information from different sources in the melting seasons 2017 and 2018. The mean of all the statistical measures derived from the intercomparison of the S1 wet snow products with these different reference snow information (Section 4.1) are summarized in Table 4.1.

Table 4.1: Mean statistical measures from the validation of the wet snow products with different reference information.

S1 Wet snow vs	*Grid spacing for comparison*	*# comparison pairs*	*Recall*	*Precision*	*False Alarm Rate*	*F-score*	*Accuracy*
FSC(S) ≥ 90%	100 m	58 333 312	0.58	0.82	0.08	0.64	0.80
FSC(K) ≥ 90%	100 m	58 333 312	0.56	0.84	0.07	0.63	0.79
FSC(D) ≥ 90%	100 m	58 333 312	0.57	0.84	0.07	0.64	0.80
SD and LST	100 m	659	0.08	0.15	0.02	0.10	0.95
E-codes and SD >5cm	100 m	4727	0.28	0.55	0.01	0.37	0.95
WSFS SWE & melt rate	100 m	167 914 925	0.59	0.32	0.21	0.41	0.76
HBV LWC > 5% – multi-temporal analysis	1 km	97404448	0.46	0.58	0.09	0.51	0.82
HBV LWC > 5% – single day analysis	1 km	58123540	0.16	0.58	0.03	0.25	0.79
HBV LWC > 5% – diurnal variability analysis	1 km	58913284	0.14	0.69	0.03	0.24	0.73

The mean overall accuracy is well above 70% for all validation and comparisons approaches, and the mean false alarm rate is for most approaches smaller than 10%. Only for the comparison with the modelled melt rate for Finland, the FAR is larger than 20%. But the mean F-scores, the weighted average of recall and precision, indicate significant differences, not only between the different validation approaches but also between the wet snow maps from S1 and all used reference data sets. The validation results with the different reference data are further discussed in the following sub-sections.

4.2.1 Wet snow validation with high resolution reference snow maps

The intercomparisons of the wet snow maps with the reference snow maps from satellite data (cf. Section 4.1.1) result in overall accuracies around 80% with false alarm rates of about 8% and F-scores of about 64%. The high overall accuracies are frequently driven by correctly classified snow free areas.

Additional to these measures, Cohen's κ-coefficient (Cohen, 1960) is calculated for each of these comparison pairs. The accuracies and κ-coefficients resulting from the wet snow comparison with the snow maps from individual Landsat 8 and Sentinel-2 scenes of 2017 and 2018 are shown in Figure 4.2. The accuracy is exceeding 80% in most cases for these comparisons, while the κ-coefficient is in most cases at least larger than 0.4, so following the definitions of Landis and Koch (1977), the agreement between the wet snow and the reference snow maps is moderate to substantial.

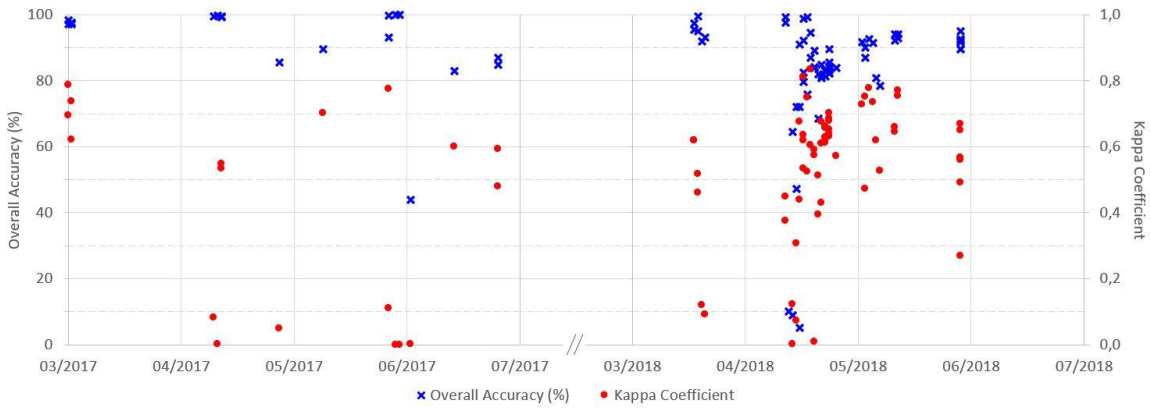

Figure 4.2: Overall accuracy and κ coefficient for S1 binary wet snow products of melting seasons 2017 and 2018, evaluated with reference snow maps from Sentinel-2 and Landsat 8 images generated with approach of Salomonson and Appel (2006) and converted to binary snow maps classifying all aggregated fractional snow cover pixels ≥ 90% as snow.

For a few cases, these measures are below 20%, indicating none or only slight agreement of the products. For most of these cases, there are three main reasons for such low values: 1) the overlap of the S1 based wet snow product and the reference snow map from the optical satellite image is small, and/or 2) there is no snow in the reference snow map, while in the S1 based product mainly agricultural areas are misclassified as wet snow, and/or 3) snow areas identified from the optical satellite data are cold and dry at the time of the S1 acquisition (mainly for descending tracks, so morning acquisitions), and are thus not matched by the S1 based wet snow product. It should also be noted that towards the end of the melting period, when the snowpack is thin and can completely melt within a few hours, only one day delay between the S1 and the reference image acquisition can result in misleading quality assessments, and results need to be interpreted with caution, ideally taking additional information (e.g. meteorological data) into account.

4.2.2 Wet snow validation with in-situ snow depth, e-codes and LST measurements

The results from the validation of the wet snow product with snow depth (SD) observations combined with e-codes and with LST, respectively, indicate that the wet snow maps identifies wet snow rather poorly (for SD & e-codes, the *Recall* is 0.28, for SD & LST, it is only 0.08; i.e. only 28% and 8%, respectively, of true wet snow cases are identified), but on the other hand does not generate false wet

snow when ground is covered by dry snow or is snow-free (*False alarm Rate* is 0.01 for SD & e-codes and 0.02 for SD & LST, i.e. only 1% and 2%, respectively, of cases classified as 'wet' are really dry snow/snow-free). *Hit Rates* are high in both cases but only because of the high number of true negatives because so many dry snow/free cases. It is a valid measure only when in-situ observations are more balanced. Here *F-score* is the best indicator, as is accounts for both Recall and Precision. As both measures used as input for the F-Score are considerably low, also the resulting F-Scores are rather low, for the validation with SD and e-codes 37% and for the validation with SD and LST only 10%.

It should be noted that the validation results with SD and e-codes are slightly hampered by the low number of true wet snow (259) cases compared to true dry snow/snow free cases (4468). This imbalance is of course non-desirable but cannot be avoided due to the limited match between SAR-acquisitions and relative sparse weather stations observations with simultaneous e-code and snow depth. The geographical locations of successful wet snow identification and misclassifications are presented in Figure 4.3.

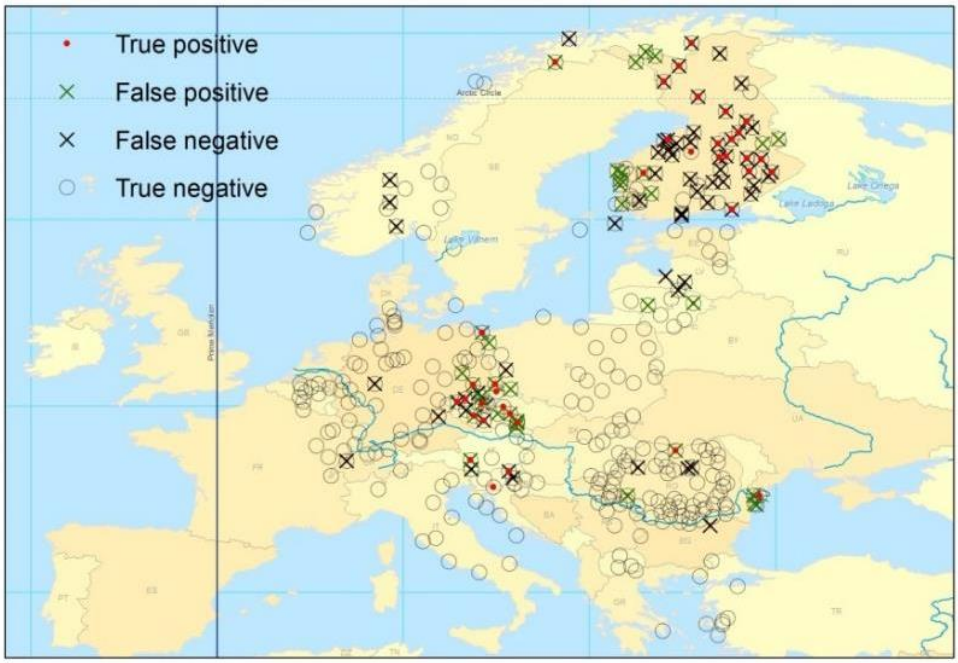

Figure 4.3: Locations of true positives, false positives, true negatives and false negatives.

The misclassifications (false positives, false negatives) do not seem to be latitude dependent; there are a lot of misclassifications at the Alps, but this is because there are also a lot of cases in general. Detection of snow presence in snow free cases (indicated by the FAR) is overall least probable. However, vice versa, snow presence is detected as snow free conditions regularly. This is likely due to the wide range of properties that snow can exhibit, e.g. variable thickness, patchiness, density. Fractional and patchy snow cover hampers the wet snow detection from S1 data.

Using in-situ data for the validation of the wet snow product, including e-codes (only for Finland) and Snow Depth and Air temperature (available at weather stations for the entire Europe) seems to provide different results. This implies that i) the product does not perform so well at European level but does a good job in Finland) or ii) the validation concept with weather station data must be adjusted.

The SAR wet snow detection can identify wet snow if the snowpack is deep enough and the ground is completely covered by snow within the pixel. Based on the comparison with in-situ data it seems that most of the wet snow cases remain undetected but on the other hand snow-free/dry snow cases are not falsely interpreted as wet snow i.e. false alarms are not produced. However, there are weakness in-situ data and in the wet snow product itself that prevents us to draw final conclusions as to the performance of wet snow detection:

- there is no certain information available on the real status of snow. This conclusion concerns both Land surface temperature fields and e-codes.
- The use of LST maps from MOIDS data is limited due to i) frequent and spatially extensive gaps in the data due to the clouds and ii) difficulty in the determination of applicable threshold for classifying snow as 'wet'.
- e-code is an ambiguous measure since it is observer-dependent and determines not just wet snow but also compact snow which may be wet or dry.

The fact that forested pixels are masked in the wet snow product limits the number of comparison pairs drastically. In areas like in Finland, in-situ sites are mostly in forested areas (although actual observation may be taken in forest opening), thus reducing the number of comparison pairs in this region remarkably.

4.2.3 Wet snow validation with hydrological model output

4.2.3.1 Finland

For the validation of the binary 100m wet snow product using modelled SWE and melt rate in Finland, combined to provide the information on wet snow, only wet snow maps generated from ascending S1 tracks, i.e. afternoon acquisitions, of the melting season 2017 are used.

The comparison results indicate that the ability of SAR wet snow product to identify wet snow (using modelled melt rate ≥2mm/d and SWE ≥60mm to generate the reference) is only moderate; the recall is 0.59 i.e. 59% of modelled wet snow cases are found. On the other hand, the product tends to produce false wet snow identifications at dry snow/snow free conditions (false alarm rate is 0.21 i.e. 21% of modelled dry snow/snow free cases are incorrectly identified as wet snow). However, due to the imbalance of number of reference wet and dry/snow free cases, the result is statistically not reliable.

Since the SAR-based wet snow detection method is not capable of identifying patchy snow cover, it is important that reference data represents full snow cover situation. SWE ≥60mm may represent also

patchy snow in some conditions, depending on the snow season's local maximum SWE. In most cases however, it should be quite representative value for full snow cover. Nevertheless, we analysed the behaviour of *Recall*, *False Alarm Rate* and *F-score* for alternating SWE-thresholds. The result is shown in Figure 4.4 where these parameters are presented as a function of increasing SWE threshold for generating reference wet snow cases. It is clear from the figure that the higher the SWE, the better is the capability to detect wet snow cases, i.e. *Recall* increases towards higher SWE. At the same time, *FAR* is also slightly for increasing, causing the slight reduction of *F-score*.

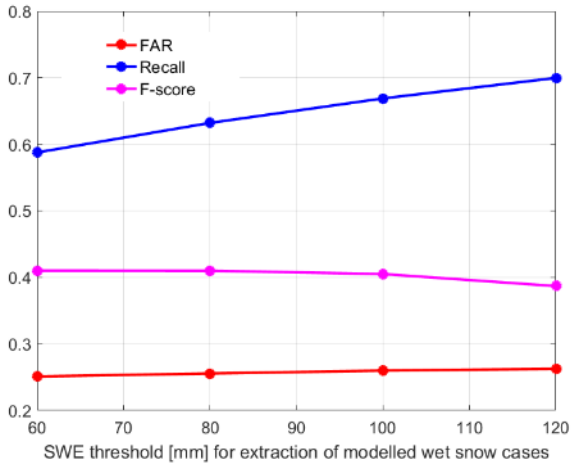

Figure 4.4: FAR, Recall and F-score for binary wet snow product with increasing SWE threshold applied to reference melting snow model.

We also detected the wet snow product's capability to detect thin wet snow cover (SWE < 60mm and melt rate ≥2mm/d). These cases certainly include also patchy snow cases in addition to full snow cover. 14 181 187 such reference cases were extracted out of total number of 226 767 397 cases. Wet snow product found 9.5% of these cases, i.e. *Recall* is 0.095. This was expected as like mentioned above, the method is applicable only to full snow cover.

4.2.3.2 Norway

From the validation of the S1 based wet snow product aggregated to 1 km grid with the hydrological model output for Norway for the years 2017 and 2018, illustrated in Figure 4.5, we observe that the overall accuracy is quite good in the melting period (DOY 120-200, April – July). During the winter period (October – March) the overall results are very fluctuating, and the overall wet snow fraction do not in general correlate well with the model.

The main reasons for this behaviour are several:

- In certain dates / periods the wet snow maps from SAR do not compare well with the model. The main reason for this is that the LWC model with the threshold we apply (5%) in general suggest a much larger area covered by wet snow than is detected by the S1 based product.

- Another reason for underestimation of wet snow area could be that the LWC product is an average over the whole day, whereas S1 detects wet snow in the morning and afternoon. During the winter period the morning can often be the coldest period, while the late afternoon seldom is the warmest time of the day. Hence, there is a bias in the diurnal sampling of the two products.
- By using the NVE product with 3 hourly sampling we saw that there is a consistency between the diurnal variability of the S1 wet snow product.
- In the S1 based wet snow products forested areas are masked. For areas with tree cover not masked by the auxiliary data set, SAR underestimates wet snow, while the frequency of wet snow in the LWC product often is higher than in the mountains during the winter period.

The multi-temporal concept of wet snow detection is not sensitive towards rapid changes in temperature (e.g. sudden rise above 0°C with onset of melting) and may lead to significant underestimates of wet snow.

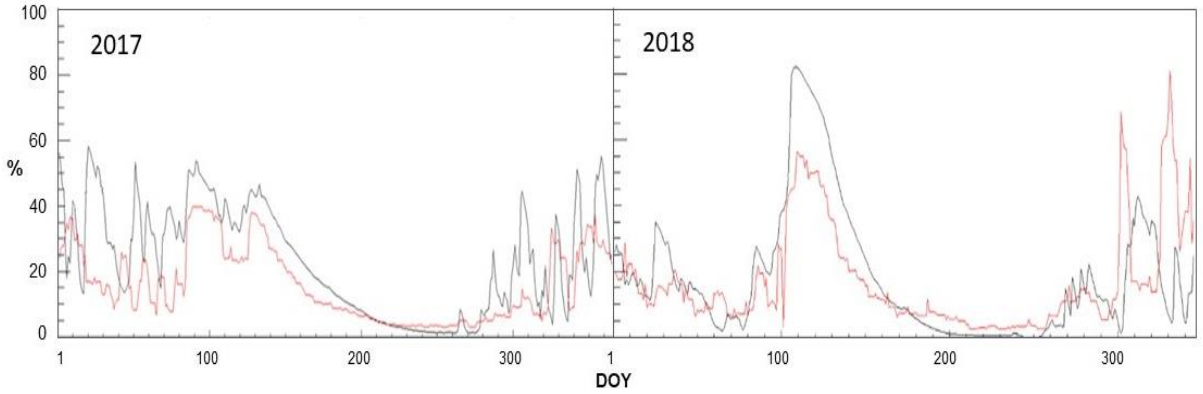

Figure 4.5: Multi-temporal analysis of daily wet snow fractions from S1 (red) aggregated to 1 km grid size (>10%) and the LWC (>5%) from the HBV model (black) at 1 km grid size for southern Norway for the years 2017 and 2018.

The results from the comparison with the hydrological model for LWC show that the accuracy of the S1 based wet snow maps is good in the spring melt period, but in the winter season there are larger differences between the model and the S1 observations. In general, we believe that wet snow is underestimated during the winter period, but it is also unclear whether the HBV-model over-estimates wet snow. Our study also shows that the diurnal variability in morning and afternoon acquisitions correlates well with the model.

5. SOFTWARE IMPLEMENTATION

The SAR Wet Snow Mapper and the Generate Reference Image are custom extensions to the existing SNAP version 7.0 framework tailored to the wet snow mapping procedure at small scales. The extensions have been developed in Python and are integrated into SNAP using the snappy Python module. Additionally, Maven was used to package the software code into a plugin archive which can be shared among users. The archive can then easily be installed in SNAP through the Plug-in interface, accessible via the menu Tools → Plugins.

After successful installation, the program is available via the menu Radar → SAR wet snow.

The "SAR Wet Snow Mapper" contains a help section providing general information on the wet snow detection, including the reference to Nagler *et al.* (2016), describing the algorithm in detail. Further, the individual steps within the program are outlined. Previews of the modules "Generate Reference Image" and "SAR Wet Snow Mapper" in the SNAP framework are shown in Figure 5.1 to Figure 5.3.

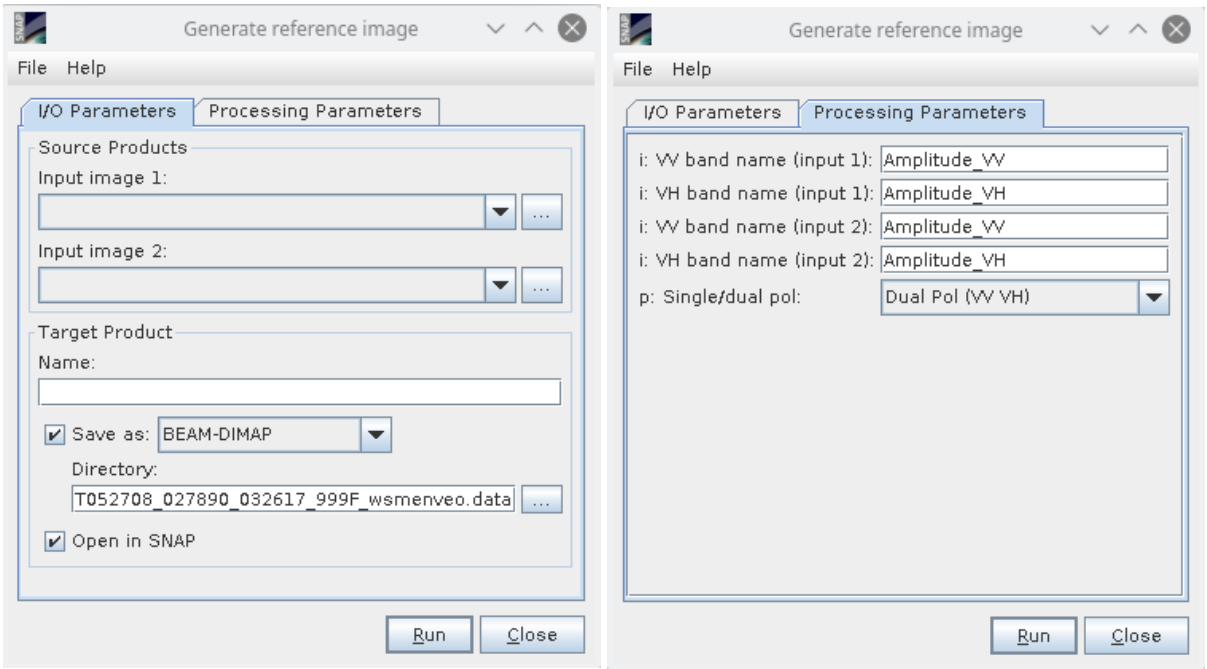

Figure 5.1: Previews of SNAP tool for generating the reference image required as input for the "SAR Wet Snow Mapper" module. Left: Input/Output Parameters specifications. Right: Processing Parameters specification.

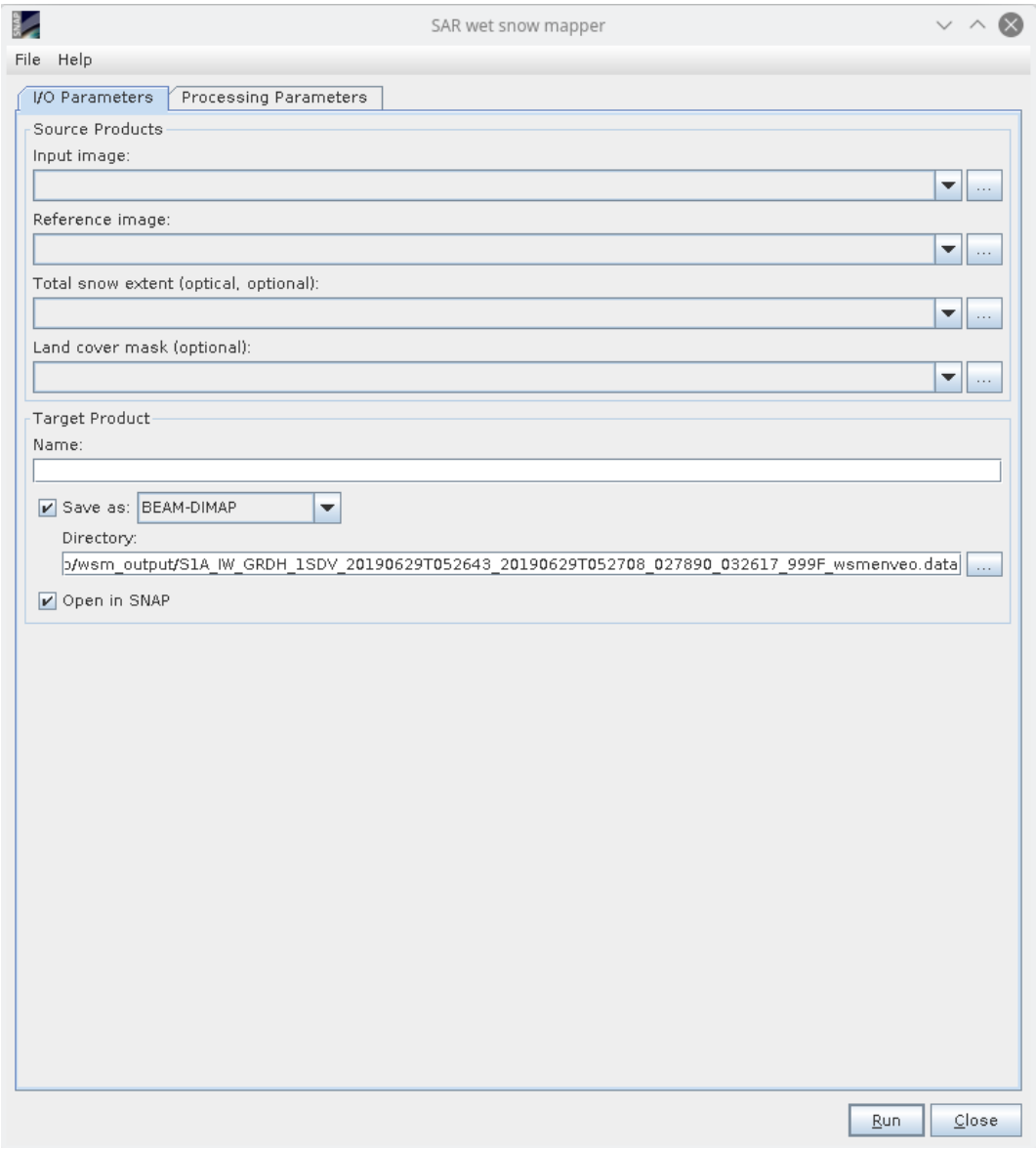

Figure 5.2: Preview of main window of “SAR wet snow mapper” implemented as SNAP tool. Input image specifies the S1 SAR scene; Reference image is the map resulting from the tool “Generate reference image” shown in Figure 5.1; Total snow extent (optical, optional) allows to add a snow map generated from an optical satellite sensor; Land cover mask (optional) allows to mask any land cover types such as open water or forested areas. Target product specifies the file name of the output product. The directory to save the product and the file type of the product can be changed. The content of the tab “Processing parameters” is shown in Figure 5.3.

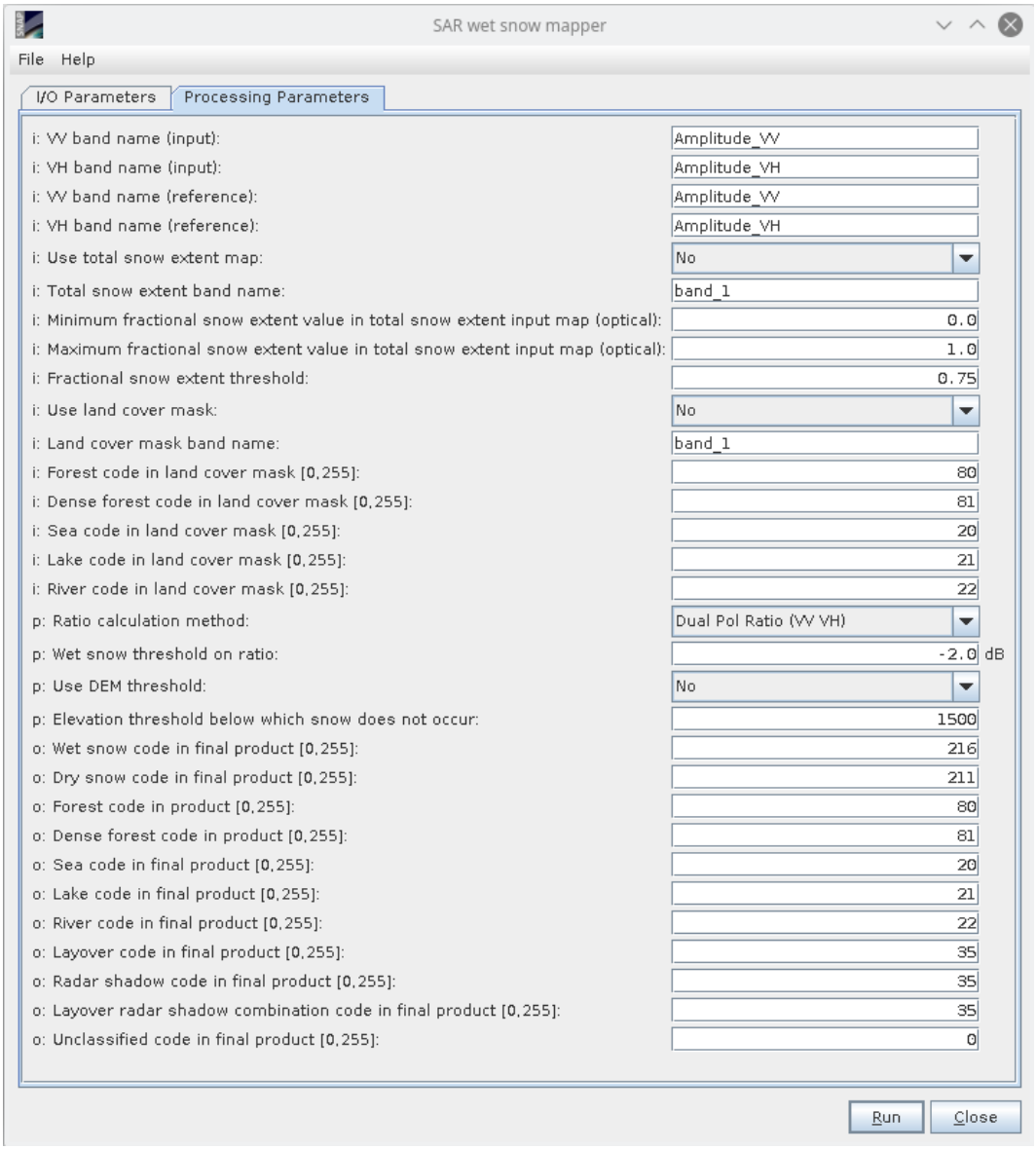

Figure 5.3: Processing parameters to be set or changed for the "SAR Wet Snow Mapper". Digital coding in this example is set according to the EU FP7 CryoLand coding, available at http://cryoland.enveo.at/downloads/CryoLand4Newbies/CryoLand4Newbies.pdf, Appendix B, but can be changed within the given allowed value range according to a user's need.

6. ADVANCING SAR AND COMBINED SAR AND OPTICAL SNOW PRODUCTS

In this section, we identify and discuss options for improving the SAR wet snow products, including exploitation of synergy with medium resolution optical snow products and with snow process modelling. On the sensor side, the focus is on Copernicus S1 SAR data and Sentinel-3 SLSTR /OCLI derived snow products.

- Detection of snow melt extent in forested areas: In the current version for wet snow detection the forested areas were masked out using maps of forest cover from other sources. To study the feasibility of detecting melting snow in forests, a radiative transfer model for simulating backscatter from forested snow-covered terrain can be applied. A suitable model was developed by Macelloni *et al.* (2012) and later applied by Montomoli *et al.* (2016) in preparation for the CoReH2O mission to assess the feasibility for retrieving SWE in forested areas from X- and Ku-band backscatter measurements. In the forest model, the canopy is divided into several horizontal layers over snow-covered terrain. Each layer contains different groups of scatterers, and each group is assumed to be composed of identical scatterers with a certain density. The radiative transfer equation is solved by iteration for the first-order (i.e., single-scattering) backscattering coefficients, accounting for direct scattering from the (snow-covered) ground and from the vegetation, as well as for interactions between snow or ground and vegetation. In sparse forests, as is the case for many boreal forests, the model considers tree shadow effects to quantify the percentages of direct and ground/vegetation backscatter contributions. The backscatter simulations show that tree height and biomass and critical parameters for assessing the feasibility of obtaining a suitable signal from the snow on ground.

  A sensitivity analysis with such a model will help to check the capabilities and limitations on detecting wet snow in forested areas. The modelling results need to be evaluated with experiments in boreal forest regions. In dense forests, the masking effect of the canopy is probably too strong and will prohibit any reliable detection of wet snow. The limit for the feasibility of wet snow detection in dependence on the forest density (and tree height or biomass, if available) needs to be assessed. Main input data for such a study would be S1 SAR data, optical satellite data (to check if snow is present) and digital maps of forest extent and properties, e.g. Copernicus High Resolution Layer: Tree Cover Density.

- Towards daily coverage by the Pan-European SAR melt extent product: Due to the high temporal and spatial variability of snow melt, daily sequences of melt extent products would be of great benefit for hydrology, for water management, as input for numerical meteorological models. The 2-satellite S1A and B constellation requires 3 to 5 days for a complete coverage of Europe. There are two scenarios towards achieving daily sequences. One option is the integration of the S1 snowmelt product in the land surface/snow component of mesoscale numerical meteorological models. Several mesoscale models include a snow process model that simulates and forecasts the melting state of the snow cover in sub-daily time steps. Assimilation of satellite products in these

models can be used for initialization and correction of the numerical snowmelt forecasts, thus achieving an improved integrated snowmelt product in close time steps.

Another option is the exploitation of an enlarged ensemble of SAR satellites providing input data for snowmelt retrievals. This will include the integration of the S1C satellite into the Sentinel constellation after the launch scheduled for 2022/23. The orbit scenario for the enhanced S1 mission is currently in discussion. One option under consideration by ESA and Copernicus is to operate the A-, B- and C satellites so that 4-day repeat-pass coverage along the same ground track is achieved. The combined utilization of data from the S1 A/B(/C) and Radarsat Constellation Mission RCM (C-band SAR) would offer an opportunity for a significant increase in the repeat coverage. The current RCM acquisition plan does not include a continuous coverage of Europe. Initial tests for the integration and added value of data from both missions could be carried out over Canada. Potentially, the coverage in comparison to S1A/B could be doubled, and the temporal resolution driven to one or two days. As the RCM and S1 systems have different modes and standard imaging geometries, radiometric terrain correction would be necessary that is tailored to the individual acquisitions. If routine acquisition by RCM over Europe can be achieved, the combination of S1 with RCM would offer a sound basis for a Copernicus Pan-European snow services on daily snow melt extent.

- Towards integration of new CEOS analysis ready data for land (CARD4L) products. CEOS has been developing new analysis ready data for land products with the aim of standardising processing steps such as radiometric terrain flattening procedures across multiple sensors. Examples are given in Figure 6.1.

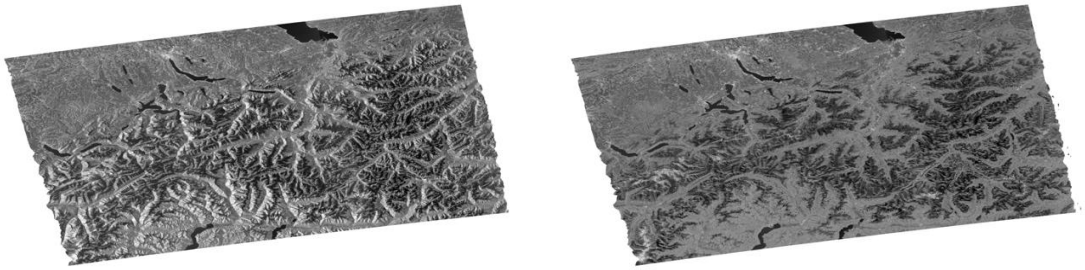

Figure 6.1: Radiometric Terrain Flattening applied to S1 data in the European Alps: (left) Geometric Terrain Correction (GTC), (right) Radiometric Terrain Correction (RTC) (Small, 2011).

- Multi-track backscatter composites. An example of a backscatter composites calculated by automatically producing terrain-flattened gamma nought backscatter estimates based on all tracks available (including ascending + descending) within a defined temporal window is shown in Figure 6.2. Three time-periods are included, with late Feb, early April, and early May shown in

red, green, and blue channel respectively. Large cities and high peaks where snow remained dry in all periods are shown as white. Low elevations began melting in April/May, so were relatively high in Feb, and appear red. Higher elevations only began melting in May, so these regions had high backscatter in February and April, and appear yellow (red+green).

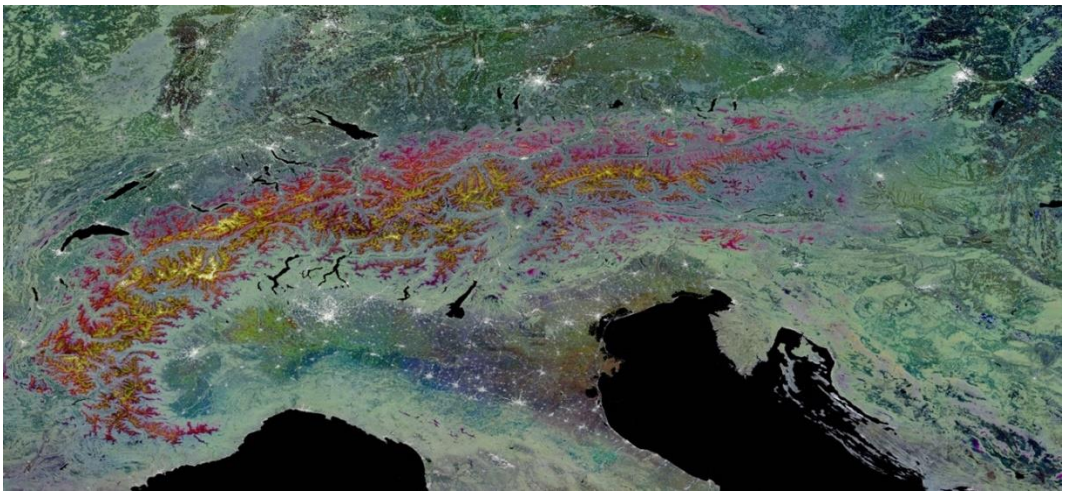

Figure 6.2: Multi-temporal Alpine S1 VH-pol. composite RGB overlay after (Small *et al.*, 2021) illustrating changes in backscatter from February through April to May 2018.

- Monitoring of transient melt/freeze events: The recording of melt/refreeze events during the snowmelt period is of importance for estimating the runoff supplied by drainage from the snowpack and for quantifying surface/atmosphere exchange processes of heat and water vapour. Such events may be triggered by advection of cold air masses or by the daily cycle of the radiation balance. S1 acquires data during morning (ascending) and afternoon (descending) passes, offering the opportunity for detecting day/night changes if crossovers happen within 12 hours. Changes in the melt/freeze conditions of the top snow layer can induce changes in the liquid water content and the backscatter coefficient. The current S1 snowmelt production line merges morning and afternoon acquisition and retrieves the maximum snow melt extent within a specified period. For assessing the feasibility of detecting melt-freeze events with S1 cross-over data numerical backscatter modelling and comparisons with 12h cross-over data should be performed, as well as comparisons with snow process model output on snow surface properties. This will help to quantify the dynamic range and sensitivity of the backscatter signal in relation to the melting state. A major constraint is the currently limited S1 coverage within 12h repeat intervals. Another critical issue is understanding the geometry dependence of backscatter terrain flattening (Small; 2011) that needs to be separated from the signal related to the melting state. This effect should be evaluated by means of backscatter modelling and experimental data to check the feasibility for application in sloping terrain.
- Generation of a high-resolution snow cover and melt extent product by combination of S1 and Sentinel-2 snow products. Although an improvement in spatial resolution will increase the

uncertainty of the SAR melt extent product at pixel scale, such products are of interest for hydrological basins on regional scale in mountainous areas, in steep terrain for avalanche danger assessment and for complex land cover. The requirements for pixel size should be assessed according to feedback from the user community, considering trade-offs between pixel size and uncertainty of the backscatter signal. For hydrological models, an input 50 m grid size would usually be adequate; higher resolution products may be of interest for special applications.

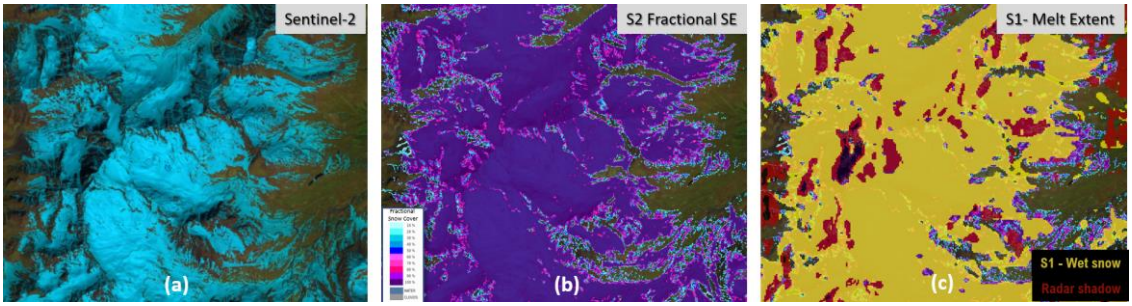

Figure 6.3: High resolution (20 m pixel spacing) fractional snow extent and snow melt area map from Sentinel-2 and S1 image, covering a high alpine area in Kaunertal, Eastern Alps of Austria. (a) Sentinel-2 image, 27 May 2017; (b) fractional snow extent map from Sentinel-2, 20m pixel spacing; (c) Wet snow extent from S1, 20 m pixel spacing, on top of Sentinel-2 FSC map.

An example of a merged snowmelt area product based on a Sentinel-2 FSC map and a down-scaled S1 wet snow product is shown in Figure 6.3 for a mountainous region in the Eastern Alps of Austria. It shows a good agreement in the snow extent of both products, some differences are observed along the snow margins with patchy snow cover. This example refers to open terrain with sparse or no vegetation. Procedures and performance for application over different terrain and land cover types should be explored. Furthermore, a strategy needs to be worked out how to bridge gaps in the availability of optical data.

- Assimilation of combined optical and SAR Snow Cover and Melt Extent products in snow process models for snow runoff modelling and forecasting: Distributed snow process models, driven by numerical meteorological grids (e.g. SnowGrid operated by the Austrian Weather Services ZAMG) and are used for snowmelt runoff modelling and forecasting. SAR-based maps of snowmelt area extent also provide valuable information for snowmelt modelling. Snowpack runoff, however, is only formed if the snowpack is ready to release liquid water, i.e. if the snowpack is isothermal at 0°C and fully saturated.

  In Alpine snowpacks up to several weeks can pass between the first occurrence of liquid water at the snow surface and the release of snowpack runoff. This means that it is less clear, how much time passes between saturation of the SAR backscatter signal so that wet snow is detected and the first release of runoff from the snowpack. An open question is how to relate the SAR based wet snow product, that indicates melting of snow (presence of liquid water in the snowpack), to

the appearance of the runoff from the snowpack and to the temporal sequence of drainage. Significant advancements on this issue can be expected from the development of dedicated data assimilation procedures for the utilization of satellite snowmelt time series in snow process models, paying particular attention to the start of melting phase and the sequence of ongoing melting and occasional transient refreezing events.

- Repeat pass InSAR SWE retrieval: Due to the reduced impact of temporal decorrelation L-Band is the preferred frequency for InSAR SWE retrieval. This method works for dry snow only. C-Band SAR can support the retrieval by detecting melting snow, thus helping to avoid misinterpretation of the L-band SAR data in which the melt-related backscatter signal is rather faint. Several L-Band SAR missions are in orbit or in the planning state, including ROSE-L as one of the Copernicus expansion missions.

7. SAR CAPABILITIES FOR NEW SNOW PRODUCTS

7.1 SAR application for retrieving snow liquid water content

When snow becomes wet, the dielectric losses of snow increase significantly, causing a large decrease in the penetration depth and of the backscatter coefficient. In the C- to Ku-band range, the one-way penetration depth for intensity of snow with liquid water content (V_w) of 2% by volume is on the order of one wavelength. Radar backscatter signatures of wet snow depend on one hand on sensor parameters (frequency, polarization, viewing angle), and on the other hand on several snow properties (Shi, 2008; Rott *et al.*, 2018).

A main parameter for backscatter intensity of a wet snowpack is the liquid water content, but also the snow density, the particle size distribution, the shape of ice and water inclusions and the surface roughness play a role. The specific impact of these parameters varies with radar frequency. Effects of surface roughness and grain size on backscatter decrease with the radar wavelength. During melting, the presence of liquid water in the snowpack directly affects the grain size, the grain shape and the density of the pack (Pomeroy and Brun, 2001). During melt, the snow undergoes a rapid metamorphism that leads to growing and rounding of the grains and an increase in the snow density.

Methods for the retrieval of V_w from SAR data are still in experimental stages. Regarding further developments on the use of S1 data for observing and monitoring the liquid water content of snow, the discrimination of wetness classes, as defined by the International Hydrogeological Program (Fierz *et al.*, 2009), would offer significant added value for hydrology and water management applications. The main classes of the wetness index are (i) moist snow, V_w = >0 to 3 %, (ii) wet snow, V_w = 3% to 8%, (iii) very wet snow V_w = 8% to 15%. Possibly, half-index steps may also be achievable, although this may not be the case for wet and very wet snow because of the decreasing sensitivity of changes in backscatter versus liquid water content. It is also of interest to explore the use of dual frequency data (in particular C- and X-band) although the requirement of temporal coincidence may be a problem.

7.2 SWE Retrieval using Repeat Pass InSAR

Differential repeat pass interferometry (DInSAR) using spaceborne synthetic aperture radar (SAR) data offers a physical based method for mapping the snow water equivalent (SWE). The method exploits the path delay of a radar signal propagating through a snow layer (Guneriussen *et al.*, 2001) and is suitable for measuring the change in SWE accumulating on a ground surface or on top of an existing snowpack. The radar should operate in a wavelength for which the absorption and scattering losses in the snowpack are small so that the main scattering contribution comes from the snow/ground interface. In the case of dry seasonal snowpack (up to some meters in depth) this is the case for C-band and L-Band data. Therefore, the method is relevant for several satellite missions e.g. S1 (C-Band), Hydroterra (ESA EE10 Candidate mission; C-Band) and several current and planned L-band SAR missions (ROSE-L, SAOCOM, NiSAR, ALOS PALSAR 4).

L-Band is the preferred frequency for SWE retrieval using InSAR, as it is less sensitive to temporal decorrelation due to snow fall. The potential of the method is currently being investigated using ALOS PALSAR-2 images with (14 day intervals) acquired over the test area Engadin, which is carried out in preparation for the Copernicus Expansion Mission ROSE-L (which will provide 6 day repeat acquisitions). The method is also suitable for Argentinian / Italian SAOCOM SAR mission (C-Band SAR; 16 days repeat cycle) and the upcoming NASA / ISRO NiSAR mission (planned for launch 2022/23).

Repeat pass InSAR enables a physical measurement of changes of snow water equivalent and requires continuous repeat pass acquisition during the winter season to track the evolution of the winter snowpack. It works for dry snow only and is not suitable for melting / wet snow and in forested areas. Temporal decorrelation is the major limitation for this method. According to current knowledge, C-band SAR decorrelates within 24 hours during snow fall (depends also on the amount of snow; Luzi *et al.* 2009). Therefore, the estimation of SWE is proposed as one of the land cryosphere parameters for the Earth Explorer 10 Candidate Missions Hydroterra. Hydroterra is a Geosynchronous SAR mission capable of providing time series of SAR images with a 12 hour repeat cycle only. As a Geosynchronous SAR, Hydroterra will acquire data over a limited area of the earth, primarily Central and Southern Europe and Africa depending on the application.

Another opportunity is the upcoming integration of S1C (scheduled for launch in 2021/22) into the current S1 constellation. Four options of S1 constellation with 3 satellites are proposed, namely (i) S1A, B and C in 12 days repeat pass orbit, shifted by 4 days (providing repeat pass observations using all 3 satellites on day 0, 4 and 8), (ii) S1C operating between S1A and S1B operating in actual orbit (providing acquisitions on (day 0, day 6 and day 9 alternatively day 3), (iii) S1A and S1B in current orbit, S1C with 1 day interval behind S1A, (iv) S1A and S1C in loose formation operating in pursuit monostatic mode. For InSAR SWE retrieval, the option (iii) with a 1-day interval would be of interest. Note that the different options for integration of S1C into the S1 constellation are currently in discussion.

7.3 Application of SAR backscatter data for Snow Depth and SWE

Since the early 1980s, extensive theoretical work and many experiments with ground-based, airborne and satellite-borne sensors have been conducted in order to explore the use of SAR backscatter intensity data for monitoring SWE and snow depth (SD). The studies focus on C-band to Ka-band frequency range. The use for sensing volume properties of snow is confined to dry snowpack because of the high absorption losses of wet snow limiting the sensing depth to less than a wavelength.

The key problem for inverting measurements of radar backscatter in terms of SD and SWE is the separation of the impact of snow mass and/or depth versus the impact snow microstructure (grain size distribution, grain shape, bonding, clusters, snow density, stratification). Direct solutions of the inverse problem for retrieving SWE and SD from a given set of backscatter measurements are not unique. Besides, uncertainties in the measurements and/or inversion model may cause large variations in the solution.

The selection of suitable SAR frequencies for observing snowpack properties has to consider on one hand the capability of penetrating a snowpack of substantial thickness, on the other hand the expected strength of the scattering source for obtaining a reliable return signal from the snow volume that is suitable for inversion. In respect to these requirements the Ku-band frequency range offers the best performance regarding seasonal snowpack. The use of Ku-band SAR for SWE monitoring has been extensively studied for the preparations of the Earth Explorer 7 Candidate Mission CoReH$_2$0 (Rott *et al.*, 2010; 2018), and is now going on in preparations for the Chinese WCOM mission (L- C- Ku- Band SAR mission; Shi *et al.*, 2016) and the dual-frequency Ku-band SAR mission of Environment Canada and the Canadian Space Agency (Derksen *et al.*, 2019).

At ***C-band,*** the backscatter signal of dry seasonal snow is largely dominated by the contribution of the underlying ground. C-band scatterometer measurements over Alpine snowpack show that both the co-and the cross-polarized backscatter coefficients are approximately constant throughout winter as long as the snow is dry, in spite of a major increase of snow depth (Strozzi *et al.*, 1997; Strozzi and Mätzler, 1998). However, changes in the physical state of the ground below the snowpack are of relevance for the backscatter signal of the snow/ground medium.

The use of this soil signal for SWE retrievals was investigated by Bernier and Fortin (1998) who developed a model that links the C-band backscattering coefficient to physical parameters of the snowpack and the underlying soil. Models and experimental data show that in the case of dry snow, the backscattering intensity is dominated by soil surface scattering. With decreasing freezing depth, the soil's backscatter is decreasing. The thermal resistance of the snowpack is a main factor for the amount of freezing and the freezing depth. For certain conditions (shallow snow cover, low temperatures, well constrained soil properties), Bernier and Fortin found a logarithmic relationship between the backscatter ratio between snow-covered versus snow-free surfaces and SWE. This is due to the inverse relation between the thickness of the snowpack and the freezing depth in soil. The possibility for using this relation to estimate SWE for shallow snow was demonstrated with a limited C-Band SAR data set over agricultural soil in a test site in southern Quebec, Canada. Tests with C-band SAR data of other regions with different ground properties and deeper snowpack were not promising.

Lievens *et al.* (2019) proposed an empirical method for estimating the snow depth at 1 km resolution over mountainous terrain at about 2-week time steps using the co- to cross-polarisation ratio of S1. The method presumes extensive temporal and spatial pre-processing of S1 SAR data before applying the change detection of the ratio for deriving snow depth. The S1 data pre-processing procedures include geometric terrain correction (GTC) without radiometric terrain flattening, spatial averaging of the original 5 m x 20 m backscatter data is applied followed by geocoding onto a 1 km x 1 km grid. Furthermore, the backscatter values are re-scaled by applying a "static bias" to account for incidence angle effects of backscatter. The static bias was derived for each individual orbit against the average backscatter values calculated over all tracks and all orbits, irrespective of the observation angle, surface type and properties, not differentiating dry snow, wet snow, forested and unforested areas and other surface types. The authors mention that they apply outlier removal; details on this (critical) procedure were not communicated. Finally, all S1 A and B data of ascending and descending orbits of

a 12-day period are merged to form a backscatter map that is used for deriving snow depth using a simple empirical relation, being applied to any snowpack type and snow cover region.

The essence of the procedure is based on change detection using the S1 $\sigma^\circ_{vh}/\sigma^\circ_{vv}$ ratio in dB that is rescaled into SD applying one single scaling value:

$$SI(i,t) = \begin{cases} \max\left(0, \left[SI(i,t-1) + \frac{\sigma^\circ_{vh}}{\sigma^\circ_{vv}}(i,t) - \frac{\sigma^\circ_{vh}}{\sigma^\circ_{vv}}(i,t-1)\right]\right), & if\ SC = 1 \\ 0, & if\ SC = 0 \end{cases} \qquad \textit{Eq. 7.1}$$

$$SD(i,t) = \frac{a}{1 - b\ FC(i)}\ SI(i,t) \qquad \textit{Eq. 7.2}$$

The snow index (SI) adds up the changes in the $\sigma^\circ_{vh}/\sigma^\circ_{vv}$ ratio [in dB] as long as snow is present (SC = 1) in an external map of snow extent (IMS snow presence at 1 km^2 resolution). If the external SC = 0 then SI is set to 0. The SI value is converted to snow depth (SD) using the scaling parameter a = 1.1 m/dB, a constant value in space and time used for the global seasonal snow cover. The dimensionless scaling parameter b is used for correcting the attenuation in evergreen forests with fractional cover (FC). A constant value in space and time is used: b = 0.6. The use of single, constant parameters for relating backscatter data to SD and forest attenuation of the global snow cover contradicts the complexity of signal interactions with snow-covered ground as known from theory and extensive experimental research in different snow regimes.

Moreover, Lievens *et al.* (2019) claim that the procedure even works when the snow is wet, although theory and measurements show that C-band propagation into wet snowpack is confined to the top few centimetres. The physical basis accounting for the relation between the VH/VV backscatter ratio and SD reported by Lievens *et al.* (2019) is unclear.

Even so, it is of interest to understand and quantify the factors accounting for the temporal evolution of the C-band VH/VV ratio during the snow cover season. In a preliminary study we analysed S1 backscatter time series at several Alpine sites for which in situ measurements are available in order to assess the performance of PALSAR repeat-pass InSAR time series for SWE retrieval. The field data on snow structural properties, SWE, soil properties and meteorological parameters are as well of interest for interpretation of S1 backscatter signatures. There is no meaningful relation found between the SD measured in the field and any of the parameters VH/VV-ratio, SI and SD. However, there are temporal changes of these parameters during the snow cover season and during the snow-free period as well. Assessing the driving factors for these features requires dedicated studies on radar signal interaction with the snow ground medium in connection with field measurements.

7.4 Mapping of Diagenetic Glacier facies

Mapping and monitoring the extent of glacier facies and of temporary surface melt is of interest for monitoring and modelling glacier/climate interactions, as well as for supporting studies of glacier mass balance and the dynamic response of glaciers to changing boundary conditions. The spatial extent of the various facies types on a glacier and their temporal variation is also an important climate indicator.

The C-band, X-Band and Ku-band radar backscatter signal of glaciers and ice sheets is closely linked to the diagenetic glacier facies. These are distinct zones revealing characteristic morphological features of the near-surface layers of snow (firn) and ice related to accumulation, ablation, and metamorphic processes. Diagenetic glacier facies can be characterized by means of distinct radar backscatter signatures and by in situ observations of snow morphology (Floricioiu and Rott, 2001; König *et al.*, 2004; Partington, 1998).

The classification of diagenetic facies on glaciers is based on empirical thresholds of backscatter intensity (σ°) in SAR images of the winter period (dry snow). In summer, the signal of melting snow (low σ°) dominates in the percolation zone which makes it easy to discriminate snow covered surfaces and bare ice (Nagler, 1996; Floricioiu and Rott, 2001). For mapping and monitoring of melting snow areas on glaciers by means of SAR, the same method (based on change detection in multi-temporal SAR data) is applied as for mapping snow melt areas in ice-free terrain (Nagler and Rott, 2000, Nagler *et al.*, 2016). Applications of this technique for mapping melting areas on Alpine glaciers have been shown for C-band and X-band SAR data.

The C-band algorithm for mapping of **glacier facies** has significant potential for operational applications using time series of S1 SAR data. It can be applied to time series of S1 SAR data to generate time series of the extent of melting snow area on a glacier through summer (Nagler 1996, Floricioiu, D. and H. Rott, 2001; Heilig *et al.*, 2019). This information is required as input for modelling and forecasting glacier runoff, applying models driven by numerical meteorological data. Focus on operational applications would be regions where melt water of glaciers is a main source for water supply, human consumption, agriculture, hydropower generation etc. The satellite product on glacier facies is as well of scientific importance for monitoring and modelling glacier mass balance and glacier response to climate change.

7.5 Mapping of avalanche release and debris areas using Sentinel-1

Satellite-borne SAR data is very suitable for monitoring of avalanche activity over large regions. SAR images from the S1 constellation are currently preferable, due to the large footprint of S1 data (250 x 150 km), the relative high resolution (20 x 20 m) and the high revisit frequency. The S1 constellation covers all snow-covered mountain areas worldwide, except for the Transantarctic Mountains. One can expect a revisit frequency of maximum 12 days, however, in many mountain areas, images of similar geometry and orbit can be acquired every 6 days, and even more frequent when multiple geometries

are used. With increasing latitude, the revisit frequency decreases to daily coverage. There is thus high potential for consistent and reliable avalanche activity monitoring over entire winters in large regions.

An automatic avalanche detection system, based on thresholding of temporal backscatter change and subsequent segmentation was tested in Northern Norway during the winters 2014 – 2019 (Eckerstorfer *et al.*, 2019). Based on the spatial resolution of S1, middle to large avalanches were detectable, with detection accuracy increasing with avalanche size. Moreover, wet snow avalanches were more likely to be detected. But SAR borne avalanche detection suffers from high false alarm rates at times, due to the dynamic nature of snow transferring from wet to dry conditions in the images that constitute the change detection pairs. Another challenging fact is that both, avalanches and their surrounding consist of snow, and it cannot be deduced from the SAR image if there is dry snow or no snow on the ground. These facts can lead to false alarms from features in the mountain landscape that exhibit relative backscatter change over the course of a couple days and resemble avalanches in their shape (e.g. talus slopes, avalanche fans, debris flow tracks).

Further developments in automatic avalanche detection using neural networks is ongoing. A few studies have emerged recently, revealing the potential in using neural networks for avalanche segmentation (Bianchi *et al.*, 2019; Kummervold *et al.*, 2018; Sinha *et al.*, 2019; Waldeland *et al.*, 2018).

8. AVAILABILITY OF ENVISAT ASAR DATA FOR GENERATING A HISTORIC TIME SERIES OF WET SNOW PRODUCTS

To generate a combined snow cover and melt extent product, SAR and optical satellite data are needed. Here we study the availability of these data sets for generating a long time series starting from 2000 onwards.

Snow extent products are derived from TERRA Modis data covering Europe every day from 24 February 2000 onwards. MODIS data are available for free and can be downloaded from NASA MODIS LAADS services. Daily MODIS snow fractional cover products with 500 m pixel spacing generated by ENVEO are available at the cryoland.eu geoportal.

Systematic acquisitions from C-Band SAR data with continental coverage and suitable for wet snow monitoring in the pre-Sentinel era from 2000 to 2015 onwards are the ESA missions ERS-2, ENVISAT, as well the Canadian missions Radarsat-1 and Radarsat-2. Table 8.1 summarizes relevant information on ERS-2 and ENVISAT ASAR. Data from ERS and ENVISAT are freely available to the public. Third party missions relevant for monitoring wet snow are Radarsat-1 (operating from 1995 to 2013), and Radarsat-2 (launched 2007 and still active). As Radarsat-2 is a commercial mission and data are not available for the project, we could not analyse archived acquisitions for Europe. For some limited areas such as Svalbard, Norway there exists data stacks for the period 2012-2014 that could be used to demonstrate applications where it is important to bridge the lack of data in the period between ASAR and S1. These data are, however, restricted under the Norwegian Radarsat-2 agreement and not publicly available.

Table 8.1: Characteristics of ESA C-Band SAR Missions ERS-2 and ENVISAT and Canadian Radarsat-1 and Radarsat-2

Mission / Sensor	*Mode*	*Period*	*Swath width*	*Approx. Resolution*
ERS-2	Image Mode	1995 - 2010	100 km	30 m
ENVISAT / ASAR	Image Mode	2002 - 2012	100 km	30 m
	Wide Swath Mode		400 km	150 m
Radarsat-1	Fine Mode	1995 - 2013	45 km	8 m
	Standard Mode		100 km	30 m
	ScanSAR Modes		300-500 km	50-100 m
Radarsat-2	Fine	2007 - present	50 km	8 m
	Standard		100 km	25 m
	Wide Fine		150 km	8 m
	Wide		150 km	25 m
	ScanSAR Narrow		300 km	50 m
	ScanSAR Wide		500 km	100 m

Focusing on the generation of historic time series of wet snow maps over Europe since 2000, we analysed the availability of the ENVISAT ASAR IM and WSM data. The coverage was analysed for the melting period February to June for the years 2002 to 2012 separately, images acquired in the period July to January of each 2002-2012 might be used as reference images. Assuming a melting period from February to June, SAR images acquired in this period are used for generating wet snow maps.

In 1 day Europe is only sparsely covered by both modes. 1 week shows a full coverage in Northern Europe (Scandinavia), the other parts of Europe are partly covered. For a period of 35 days Europe is almost fully covered by at least one acquisition, most regions are observed several times (Figure 8.1). ASAR IM acquisitions cover Europe only partly.

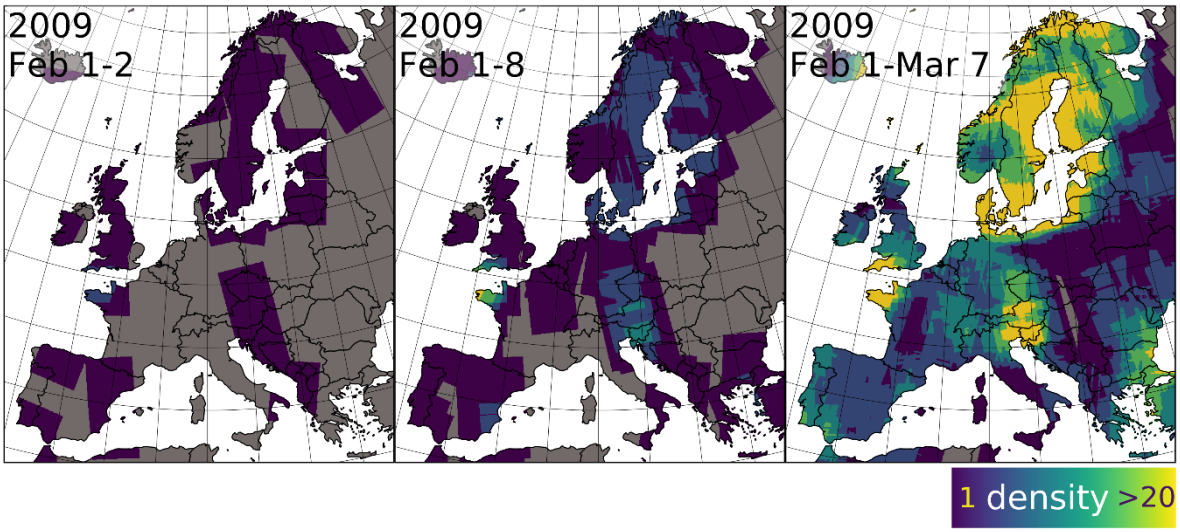

Figure 8.1: Example of the number of images (density) and coverage of ENVISAT ASAR WS mode for 1 February 2009 (1 day), 1-8 February 2009 (1 week) and 1 February to 7 March 2009 (1 ENVISAT cycle, 35 days).

Figure 8.2 shows the number of acquisitions (image density) and coverage of ASAR WSM for Europe for the melting period (1 February to 30 June) of each year 2002 to 2012. Figure 8.3 shows the number of acquisitions (image density) and coverage of ASAR WSM for Europe for the period 1 July to 1 January for each year 2002 to 2012, the acquisition may contribute to the generation of the multitemporal reference scenes. According to the image density, ASAR WSM is the primary acquisition mode for generation of the ENVISAT full mission time series wet snow products. This can be complemented by ASAR IM data to increase the temporal sampling and coverage. Although the method of SAR wet snow mapping was already successfully tested and applied to both acquisition modes of ENVISAT, some software and technical developments are needed to optimize computational costs in time series generation.

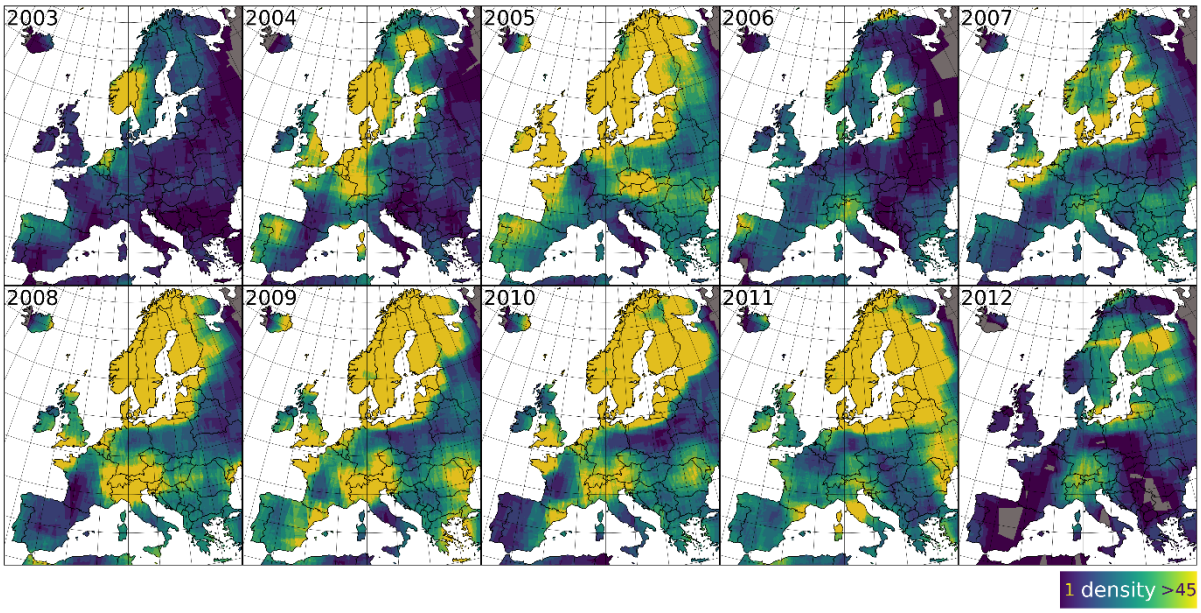

Figure 8.2: Number of images (density) and coverage of ENVISAT ASAR WS mode for the melting period (1 February to 30 June) for the years 2002 to 2012. The acquisitions can be used as wet snow images for the SAR wet snow algorithm.

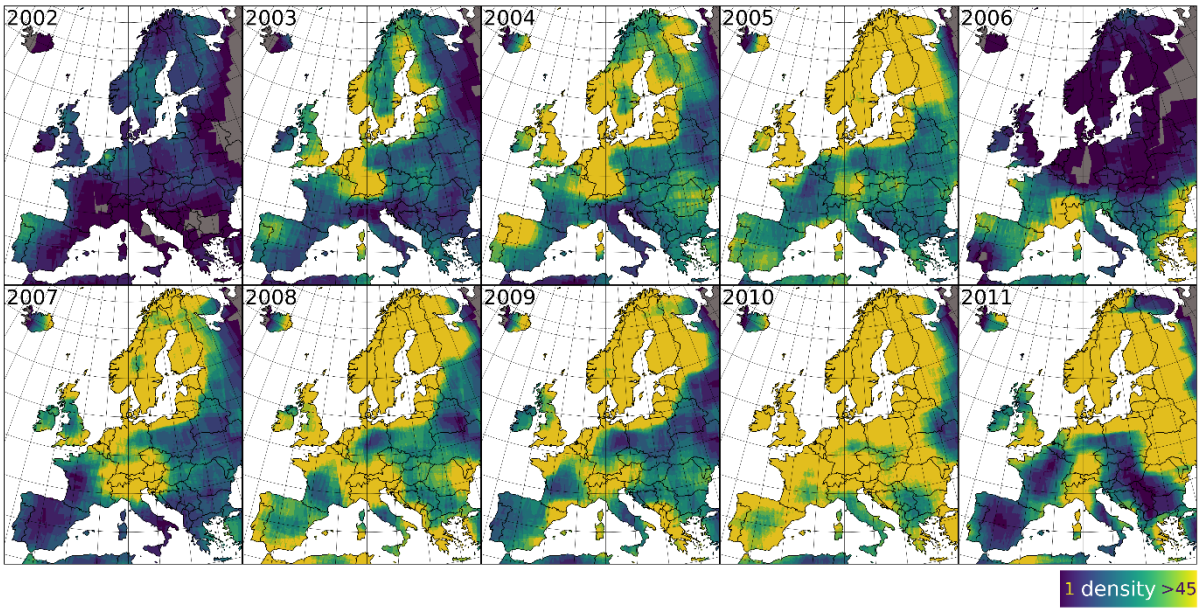

Figure 8.3: Number of images and coverage of ENVISAT ASAR WS mode for 1 July to 31 January for the years 2002 to 2012. The acquisitions can be used for generation of the reference scenes for the SAR wet snow algorithm.

9. REFERENCES

Bernier, M. and J.-P. Fortin, 1998. The potential of times series of C-Band SAR data to monitor dry and shallow snow cover. IEEE Trans. Geosc. Rem. Sens., 36(1), 226-243.

Bianchi, F.M., J. Grahn, M. Eckerstorfer, E. Malnes, H. Vickers. 2019. Snow avalanche segmentation in SAR images with Fully Convolutional Neural Networks. ArXiv191005411 Cs Eess Stat.

CEOS, 2020. Analysis Ready Data for Land (CARD4L), http://ceos.org/ard

Cohen J., 1960. A coefficient of agreement for nominal scales. Educational and Psychological Measurement, 20(1), pp. 37–46. https://doi.org/10.1177/001316446002000104

Derksen, C., J. Lemmetyinen, J. King, S. Belair, C. Garnaud *et al.* 2019. A dual-frequency radar mission concept for seasonal snow. Proc. IGARSS 2019, Yokohama, Japan, pp. 5742-5744.

Eckerstorfer, M., H. Vickers, Malnes, E., Grahn, J., 2019. Near-Real Time Automatic Snow Avalanche Activity Monitoring System Using Sentinel-1 SAR Data in Norway. https://doi.org/10.20944/preprints201910.0341.v1

Fierz, C., R.L. Armstrong, Y. Durand, P. Etchevers, E. Greene *et al.*, 2009. The International Classification for Seasonal Snow on the Ground. IHP-VII Techn. Documents in Hydrology N°83, IACS Contribution N°1, UNESCO-IHP, Paris.

Floricioiu, D. and H. Rott. 2001. Seasonal and short-term variability of multifrequency, polarimetric radar backscatter of alpine terrain from SIR-C/X-SAR and AIRSAR data. IEEE Trans. Geosc. Rem. Sens. 39(12), 2634 – 2648.

Guneriussen, T., K. A. Hogda, H. Johnson, and I. Lauknes (2001). InSAR for estimating changes in snow water equivalent of dry snow, IEEE Trans. Geosci. Rem. Sens. 39(10), 2101-2108.

Heilig, A.; Wendleder, A.; Schmitt, A.; Mayer, C. Discriminating Wet Snow and Firn for Alpine Glaciers Using Sentinel-1 Data: A Case Study at Rofental, Austria. Geosciences 2019, 9, 69.

König, M., J.-G. Winther, J. Kohler, and F. König. 2004. Two methods for firn-area and mass balance monitoring of Svalbard glaciers with SAR satellite images. Journal of Glaciology, 50(168), 116-128.

Kummervold, P.E., Malnes, E., Eckerstorfer, M., Arntzen, I.M., Bianchi, F., 2018. Avalanche detection in Sentinel-1 radar images using convolutional neural networks. Int. Snow Sci. Workshop Proc. 2018 Innsbr. Austria 377–381.

Landis, J., and G. Koch. 1977. The Measurement of Observer Agreement for Categorical Data. Biometrics, 33(1), 159-174. doi:10.2307/2529310

Lievens, H., M. Demuzere, H.-P. Marshall, R.H. Reichle, L. Brucker, I. Brangers, *et al.* 2019. Snow depth variability in the Northern Hemisphere mountains observed from space. Nature Communications, 1010:4629, https://doi.org/10.1038/s41467-019-12566-y .

Luzi, G., L. Noferini, D. Mecatti, G. Macaluso, M. Pieraccini, C. Atzeni, A. Schaffhauser, R. Fromm, and T. Nagler (2009). Using a ground-based SAR interferometer and a terrestrial laser scanner to monitor a snow-covered slope: Results from an experimental data collection in Tyrol, Austria, IEEE Trans. Geosci. Remote Sens., 47, 382-393.

Macelloni, G., M. Brogioni, F. Montomoli, G. Fontanelli: “Effect of forests on the retrieval of snow parameters from backscatter measurements”, European Journal of Remote Sensing , 45: 121-132, 2012

Mätzler, C. 1987. Applications of the interaction of microwaves with the natural snow cover. Remote Sensing Reviews, 1987 (Vol. 2), 259 – 387 (Harwood Academic Publishers).

Montomoli, F., Macelloni, G., Brogioni, M., Lemmetyinen, J., Cohen, J., Rott, H. 2016. Observations and simulation of multifrequency SAR data over a snow-covered boreal forest. *IEEE J. Sel. Topics Appl. Earth Observ. Remote Sens.*, 9(3), 1216-1228, https://doi.org/10.1109/JSTARS.2015.2417999

Nagler, T. and H. Rott. 2000. Retrieval of wet snow by means of multitemporal SAR data. IEEE Transactions on Geoscience and Remote Sensing, 38(2), 754-765.

Nagler, T., Rott, H., Ripper, E., Bippus, G., Hetzenecker, M. (2016): Advancements for Snowmelt Monitoring by Means of Sentinel-1 SAR. Rem. Sens., 2016, 8(4), 348, https://doi.org/10.3390/rs8040348

Partington, K.C. 1998. Discrimination of glacier facies using multi-temporal SAR data. Journal of Glaciology, 44(146), 42-53.

Pomeroy, J. and E. Brun. 2001. Properties of snow, in: Snow Ecology: An Interdisciplinary Examination of Snow-Covered Ecosystems, edited by: Jones, H. G., Pomeroy, D. J. W., Walker, A., and Hoham, R. W., Cambridge Univ. Press, Cambridge, UK, pp. 45–126.

Rott, H., J. Shi, C. Xiong, and Y. Cui. 2018. Snow properties from active remote sensing instruments. In S. Liang (Ed.), Comprehensive Remote Sensing, Vol. 4, pp.237-257. Oxford: Elsevier. ISBN: 978-0-12-803221-3. (https://doi.org/10.1016/B978-0-12-409548-9.10359-8).

Rott, H., S. H. Yueh, D. W. Cline, *et al.* 2010. Cold regions hydrology high-resolution observatory for snow and cold land processes. Proc. of the IEEE, 98(5), 752-765.

Schwaizer G., J. Nemec, T. Nagler, 2019. ATBD, Deliverable 4. Development and Demonstration of Synergistic Snow Products from Optical Sensors Data and Snow Models. ESA Contract No. 4000119901/17/I-EF.

Shi, J. 2008. Active microwave remote sensing systems and applications to snow monitoring. In S. Liang (Ed.), Advances in Land Remote Sensing: System, Modelling, Inversion and Application, pp. 19 – 49). New York: Springer.

Shi, J., X. Dong, T. Zhao, Y. Du, H. Liu, *et al.* 2016. The Water Cycle Observation Mission (WCOM). Proc. IGARSS 2016, Bejing, China, pp. 3430-3433.

Sinha, S., Giffard-Roisin, S., Karbou, F., Deschatres, M., Karas, A., Eckert, N., Coléou, C., Monteleoni, C., 2019. Can Avalanche Deposits be Effectively Detected by Deep Learning on Sentinel-1 Satellite SAR Images, in: Climate Informatics. Paris, France.

Small, D. (2011). Flattening Gamma: Radiometric Terrain Correction for SAR Imagery. IEEE Transactions on Geoscience and Remote Sensing, 49(8), pp. 3081–3093. https://doi.org/10.1109/TGRS.2011.2120616

Small, D., Rohner, C., Miranda, N., Rüetschi, M., Schaepman, M.E. (2021). Wide-area Analysis-ready Radar Backscatter Composites. IEEE Transactions on Geoscience and Remote Sensing, 59, 14p. https://doi.org/10.1109/TGARS.2021.3055562

Strozzi, T. and C. Mätzler , C. 1998. Backscattering measurements of Alpine snow covers at 5.3 and 35 GHz. IEEE Trans. Geosci. Remote Sens., 36(3), 838-848.

Strozzi, T., A. Wiesmann and C. Mätzler. 1997. Active microwave signatures of snow covers at 5.3 and 35 GHz. Radio Sci., 32 (2), 479–495.

Waldeland, A.U., Reksten, J.H., Salberg, A.-B., 2018. Avalanche Detection in Sar Images Using Deep Learning. Presented at the IGARSS 2018 - IEEE International Geoscience and Remote Sensing Symposium. https://doi.org/10.1109/IGARSS.2018.8517536